Assessing the impact of urban geometry on Surface Urban Heat Island (SUHI)

Jinxin Yang[1], Massimo Menenti[3,4], Zhifeng Wu[1,2*], Man Sing Wong[5], Sawaid Abbas[5], Yong Xu[1], Qian Shi[6]

1 School of Geography and Remote Sensing, Guangzhou University, Guangzhou 510006, China；Yangjx11@gzhu.edu.cn, zfwu@gzhu.edu.cn，xu1129@gzhu.edu.cn

2 Southern Marine Science and Engineering Guangdong Laboratory (Guangzhou)，511458

3 Faculty of Civil Engineering and Earth Sciences, Delft University of Technology, P. O. Box 5048, 2600 GA Delft, Netherlands; m.menenti@tudelft.nl

4 State Key Laboratory of Remote Sensing Science, Institute of Remote Sensing and Digital Earth, Chinese Academy of Sciences, Beijing 100101, China

5 Department of Land Surveying and Geo-Informatics, The Hong Kong Polytechnic University, Kowloon, Hong Kong; email: lswong@polyu.edu.hk

6 School of Geography and Planning, Sun Yat-sen University, Guangzhou 510275, China; shixi5@mail.sysu.edu.cn

Corresponding author: Zhifeng Wu, zfwu@gzhu.edu.cn

Abbreviations

SUHIIc--The difference between the complete surface temperature of reference rural areas and the complete surface temperature of urban areas

SUHIIr--The difference between the radiometric surface temperature of reference rural areas and the radiometric surface temperature of urban areas

UHII--The difference between air temperature of reference rural station and the air temperature of urban stations

Abstract

In this study, the difference in Surface Urban Heat Island Intensity (SUHII) when using nadir-viewing radiometric and complete surface temperature (T_r and T_c) was evaluated. The urban areas of the Kowloon peninsula and Hong Kong Island across Hong Kong were selected and four daytime Landsat TM data from different seasons and two nighttime ASTER data were collected to estimate the SUHII with observations of either T_r or T_c. Additionally, high spatial resolution (HR) airborne thermal images (0.2 m) observed at 12:10 noon on Oct 24 2017 were used to retrieve T_c without additional geometric information. Results based on HR data and satellite data were consistent and indicated that the geometry of the built-up space had a larger impact on SUHII when using T_c (SUHIIc) than T_r (SUHIIr). During daytime: SUHIIc decreased with higher building density, while SUHIIr showed a very slight increase with building density. Both SUHIIc and SUHIIr decreased with higher building height but the rate of decrease of SUHIIc was higher than that of SUHIIr. Both SUHIIc and SUHIIr decreased with increasing building height difference and increased with increasing sky view factor (SVF). The rate of decrease with building height difference f SUHIIc was larger than SUHIIr. The rate of increase of SUHIIc with SVF was higher than SUHIIr. During nighttime, geometry effects on SUHIIc and SUHIIr were different from daytime. Both SUHIIc and SUHIIr increased with building density, while the rate of increase of SUHIIc with building density, as well as with building height, was much higher than that of SUHIIr. Both SUHIIc and SUHIIr decreased with SVF, but the rate of decrease of SUHIIc was higher than that of SUHIIr. Both SUHIIc and SUHIIr increased with building height difference first and then remained approximately constant. We also evaluated the UHI intensity: SUHIIc was much closer to UHII than SUHIIr. Overall, the building geometry had more significant effects on SUHIIc than on SUHIIr, i.e. SUHIIc is more representative of urban climate than SUHIIr.

Key words: urban geometry, surface urban heat island, thermal remote sensing

1. Introduction

Urbanization leads to the replacement of bare soil and vegetation by impervious surfaces, which reduces the potential for mitigation of ambient temperature through evaporation and transpiration (Kuang et al., 2015; Oke et al., 1989; Oke, 1982; Shahmohamadi et al., 2010). Instead, the radiative energy absorbed by the built-up space has to be dissipated mainly as sensible heat flux in addition to the release of anthropogenic heat, warming the surface and the atmosphere (Oke, 1981; Oke et al., 1999). This makes the urban air and surface temperature higher than the rural surface temperature because more abundant vegetation in rural areas dissipates more energy through evaporation and transpiration, thus cooling both the air and the land surface. This then has an impact on the value of both the Urban Heat Island (UHI) and Surface Urban Heat Island (SUHI) indicators of urban climate. Both UHI and SUHI have many impacts on urban climate and residents, including increasing the energy consumption for space cooling and heat stress on human residents in summer (Oke et al., 2017). The UHI metrics applies air temperature measured in the urban canopy below roof-level in the urban canyons and uses rural meteorological stations as a reference (Oke, 1981; Stewart, 2011). SUHI is defined as the difference between urban surface temperature at any urban location and the surface temperature of reference rural areas (Roth et al., 1989; Stewart, 2011). Differences between urban and rural areas in the relative magnitude of radiative and convective flux densities at the land – atmosphere interface result in different air and surface temperature in urban and rural areas, thus UHI and SUHI are indicators of the difference in surface energy balance between urban and rural areas. In other words, both UHI and SUHI are indicators of the overall effect of the built-up space on the surface energy balance.

Air and surface temperature are different geophysical variables in many ways (Oke et al., 2017) and air temperature is measured by discontinuous meteorological stations. The development of thermal infrared remote sensing made available spatially continuous observations of the land surface temperature across a range of spatial resolutions and the SUHI is based on spatially detailed observations of the radiometric surface temperature captured by space- and airborne imaging radiometers (Zhou et al., 2018). Such spatially continuous data provide detailed information towards a better understanding of urban climate and its drivers. The dependence of SUHI on urban land cover has been studied often (Chen et al., 2006; Li et al., 2016; Weng et al., 2004; Yuan and Bauer, 2007). Recently, the dependence of SUHI on the geometry of the urban built-up space has also been addressed (Yu et al., 2019). The impact of shadows determined by urban geometry has been studied by Yu et al. (2019) and results showed that in Beijing the building shadow reduced by 3.16 K the temperature of the urban impervious surface in July. More generally, the effect of urban morphology on radiometric surface temperature has been studied by Huang and Wang (2019) and the results showed that the urban geometric parameters have complex effects on the 2D and 3D pattern in urban radiometric surface temperature provided by Landsat thermal images. The urban thermal heterogeneity and 3D geometry, combined with the observation direction, lead to observe thermal anisotropy (Oke et al., 2017) and studies showed that in the Toulouse city centre the change during daytime in urban radiometric surface temperature with the view angle, i.e. the thermal anisotropy, reached 10 K on summer days in 2001 (Lagouarde et al., 2012; Lagouarde et al., 2010). This severely affects mapping of radiometric surface temperature and then the interpretation of SUHI (Hu and Brunsell, 2013; Huang et al., 2016; Li and Li, 2020; Voogt, 2011; Wang and Chen, 2019; Wang et al., 2018; Zhan et al., 2012). Current studies on SUHI are based on the radiometric surface temperature observed by thermal imaging radiometers above the urban canopy without considering the impact of anisotropy (Li et al., 2016; Peng et al., 2012; Weng et al., 2004). The radiometric surface temperature is mainly related to horizontal facets, e.g. roof and road, because most imaging radiometers are designed for nadir or near nadir looking (Roth et al., 1989; Voogt and Oke, 2003; Zhou et al. (2019)).

The impact of urban geometry on the application of thermal infrared remote sensing for urban climate research was highlighted by Roth et al (1989) and then further clarified and studied systematically by Voogt and Oke (1997, 1998, 2003) (Voogt and Oke, 1998; Voogt and Oke, 1997; Voogt and Oke, 2003). Roth et al. (1989) focused on SUHI evaluated on average for a large, mixed urbanized area using low resolution AVHRR data and discussed the limitation of the application of thermal remote sensing to study urban climate. Voogt and Oke (1997) introduced the complete surface temperature and evaluated the impact of observation geometry on measured surface temperature. Voogt and Oke (1998) documented the impact of anisotropy on the thermal infrared exitance of selected urban targets and on the surface brightness temperature retrieved from data acquired by an airborne imaging radiometer. Voogt and Oke (2003) reviewed the state of the art of thermal infrared remote sensing of urban landscapes. These studies document the notion that the complete surface temperature, which captures all the facet temperatures, is a more meaningful variable for urban climate research, since it includes information on all facets.

Different facets of the urban surface contribute to meteorological processes differently and all facets of the urban surface area are involved into the urban land surface processes and energy exchange and should be considered. The experiment conducted in Hong Kong by Ng et al. (2012) showed that a green roof is ineffective to improve thermal comfort at ground level, while trees at street level are effective in cooling pedestrian areas. This means that a roof top facet may not affect the urban canopy layer air temperature near ground, while the wall or road or other near ground facets would do so. Thus, the complete surface temperature is useful to study urban climate since it provides the information required for urban climate research, e.g. to estimate sensible heat flux (Voogt and Grimmond, 2000; Yang et al., 2019) and other heat flux densities.

SUHI is an important micro-climate indicator in urban areas. The complete surface temperature may be more useful than the radiometric surface temperature to map SUHI intensity, but it has been rarely used. The difference between complete and radiometric surface temperature can reach 10 K (Allen et al., 2018; Jiang et al., 2018; Voogt and Oke, 1997). This would lead to large differences between SUHI maps generated with either surface temperature. Thus, this study is based on the theoretical knowledge of urban geometry and it applies thermal infrared image data and complete surface temperature (Roth et al., 1989; Voogt and Oke, 1997; Voogt and Oke, 2003) to map and compare SUHIs evaluated with radiometric and (estimated) complete urban surface temperature.

In order to explore the differences in SUHIs when using different surface temperatures, this study will investigate the dependence of SUHIs on urban geometric structure when using either the complete or radiometric surface temperatures towards a better understanding of the information encapsulated in SUHI.

2. Methodology

In order to study the impact of geometry on different SUHIs, satellite data acquired by the Landsat / Thematic Map (TM) and the Advanced Spaceborne Thermal Emission and Reflection Radiometer (ASTER) and the airborne high-spatial resolution (0.2 m x 0.2 m) thermal data were collected. The satellite data of Landsat TM and ASTER were used to retrieve the radiometric surface temperature using the single channel method (Eq.1) (Yang et al., 2015) and then estimate the T_c by applying the method developed by (Yang et al., 2020a) (Eq. 2 and Eq.3):

$$E(i) = \tau_i\left[\varepsilon(\mathrm{i})B\left(T_r(i)\right) + (1 - \varepsilon(\mathrm{i}))R_{at}^{\downarrow}(i)\right] + R_{at}^{\uparrow}(i) \quad (1)$$

$E(i)$ is the radiance received by a radiometer at the top of atmosphere of pixel i. τ_i is the effective transmittance of the atmosphere, $R_{at}^{\uparrow}(i)$ is the upwelling and $R_{at}^{\downarrow}(i)$ is the downwelling atmospheric radiance. In the thermal band of L5 / TM current values of these atmospheric parameters can be obtained from the NASA Atmospheric Correction Parameter Calculator (http://atmcorr.gsfc.nasa.gov/). The radiance of ASTER AST 09T product used in this study is the ground-leaving in-band radiance including the emission of surface, the reflected radiance by the surface $\left[\varepsilon(\mathrm{i})B\left(T_r(i)\right) + (1 - \varepsilon(\mathrm{i}))R_{at}^{\downarrow}(i)\right]$ and the sky thermal irradiance in band 13 of the ASTER AST 09T product can be used to calculate the downwelling radiance to retrieve the urban radiometric surface temperature (Sobrino et al, 2007). $\varepsilon(i)$is the material emissivity of pixel i, estimated as the area-weighted average of the material emissivity of component horizontal facets, e.g. roofs, roads and ground, within the footprint observed by a nadir viewing imaging radiometer (see Yang et al. (2016b) for details). $\mathrm{B}(T_r(\mathrm{i}))$ is the upwelling radiance of pixel i with radiometric temperature $T_r(i)$. $T_r(i)$ can be derived from $\mathrm{B}(T_r(\mathrm{i}))$ based on the Planck function.

The radiometric surface temperature (T_r) observed by a nadir or near-nadir viewing remote sensor over an urban canopy includes the emitted and reflected radiance from horizontal surfaces. The reflected radiance from horizontal surfaces includes a contribution from the radiance emitted by vertical surfaces that are not directly observed by nadir or near-nadir viewing remote sensors. The difference between T_r and the complete surface temperature (T_c) is caused by the urban geometry and material heterogeneity enhanced by local meteorological conditions. (Yang et al., 2020a) developed a method to estimate T_c from Tr by performing numerical experiments to generate pseudo-observations of Tr and T_c using an urban micro-climate model, i.e. the Temperatures of Urban Facets in 3-D (TUF-3D) model, This model was developed to predict urban surface temperatures under different geometric, material and meteorological conditions (Krayenhoff and Voogt, 2007). TUF-3D model has been evaluated under different neighborhood and climate conditions (Crawford et al., 2016; Krayenhoff and Voogt, 2007) and used to evaluate radiation models (Krayenhoff et al. 2014) and provide surface temperatures for remote sensing research (Krayenhoff and Voogt, 2016; Wang et al., 2020).

According to Yang et al. (2020a), the relationships between T_c and T_r can be written as:

For daytime,

$$T_c(i) = 0.913 * T_r(i) - 5.390 * \lambda_p(i) - 1.090 * \ln(F(i)) + 0.001 Kn(i) - 0.013 * \theta_a(i) + 0.139 * \theta_z(i) + 20.598, \text{ with } r^2=0.97, \text{ RMSE}=1.500 \text{ K} \quad (2)$$

For nighttime,

$$T_c(i) = 0.927 * T_r(i) + 3.455 * \lambda_p(i) + 0.184 * \ln(F(i)) + 21.320, \text{ with } r^2=0.98, \text{ RMSE}=0.690 \text{ K} \quad (3)$$

$T_r(i)$ is the nadir-view radiometric surface temperature estimated according to Eq. (1), which takes also into account the geometry of the built-up space within the footprint of the radiometer, but captures the exitance of horizontal facets only, $\lambda_p(i)$ is building density, $F(i)$ is the wall area index, calculated as the ratio of wall area to horizontal area, $Kn(i)$ is the solar irradiance onto the urban canopy(Wm^{-2}), $\theta_a(i)$ is solar azimuth angle (°), $\theta_z(i)$ is solar zenith angle (°). These parameters were selected because they are the main factors that affect the difference between T_c and T_r after evaluation of the pseudo-observations mentioned above (Yang et al., 2020a).

The method developed to estimate the complete surface temperature by Yang et al. (2020a) (Eq. 2 and Eq. 3) was evaluated using a synthetic, model – based data set and results showed it can reach good accuracy (r^2=0.97, RMSE=1.500 K for daytime and r^2=0.98, RMSE=0.690 K for nighttime). The relationships developed by Yang et al. (2020a) were developed using pseudo-observations by carrying out a large number of numerical experiments with the model TUF – 3D for a wide range of key model parameters and of atmospheric forcing variables. The method of Yang et al. (2020a), therefore, is not limited to the specific conditions applying to the image data used to evaluate and demonstrate the approach.

The method to estimate the complete surface temperature developed by Yang et al. (2020a) is only applicable to urban areas with no or sparse vegetation cover, thus we only analyzed the impact of urban geometry on SUHIIs in built-up areas without vegetation. The impact of vegetation fractional cover and structure on SUHIIs will not be analyzed in this study. This study will only focus on the impacts of building geometric parameters on SUHIIs, e.g. building height, building density, Sky View Factor(SVF) and building height difference. The building density is calculated as the ratio of roof area to lot area. The SVF is calculated for all horizontal surfaces including roofs and ground. The ratio of roof to complete area and spacing of buildings may also have an impact on the relation of SUHIIr with SUHIIc. The building density, height and SVF can account for the effects of these parameters. Thus, this study chose building density, building height, SVF and building height deviation to evaluate the relation between SUHII-s and urban geometry.

The usage of T_c estimated from T_r, retrieved from TOA radiometric data acquired by space-borne imaging radiometers, is attractive because of the spatial and temporal coverage, although the spatial resolution of current observation systems is not sufficient to capture the urban landscape with sufficient detail. On the other hand, it needs to be evaluated whether the estimated T_c correctly captures the effect of urban geometry on the urban surface temperature. To this end, we have applied thermal infrared observations at 0.2 m x 0.2 m spatial resolution to determine directly T_c. These observations were acquired by a helicopter-mounted thermal camera and flight lines were in different directions to acquire multiple observations of the same target under different view angles (Figure 1). These data allowed the direct determination of T_c for a large number of urban facets. The atmospheric and emissivity correction were conducted first by applying the thermal image process software ReseachIR provided by the Flir company (https://www.flir.cn/). The information on different facets can be obtained from different view direction (Figure 1). The HR data were gridded at 100 m x 100 m to calculate the T_c within each grid, with Tr being the temperature observed at nadir or near-nadir direction. We visually identified each facet in the grid to estimate T_c as the area-weighted mean temperature of facets observed under different directions.

"Insert Figure 1 here"

We have evaluated the two retrievals of T_c by analyzing the dependence of both retrievals on urban geometry. The relationship between SUHIIc and the urban geometry parameters was evaluated twice, i.e. using both the T_c estimated from T_r (satellite retrievals) and the T_c determined with the high resolution thermal infrared data. This objective of the evaluation was to provide insights on the impact of the two procedures to retrieve T_c on the assessment and interpretation of SUHIIc and of its dependence on urban geometry.

UHI intensity (UHII) is calculated using the air temperature observed by meteorological stations in rural and urban areas and compared with the SUHIIs based on urban radiometric and complete surface temperature. The UHII cannot be resolved with much spatial detail in this study since only a few observation stations are available, namely the three urban meteorological stations at Hong Kong Observatory (HKO), King's Park (KP) and Sham Shui Po (SSP) (Fig. 2). The mean values of SUHIIs within a 250m buffer zone around the three urban stations will be compared with UHIIs as suggested by (Yang et al., 2020b), since the highest correlation coefficient between building and air temperature was obtained when averaging the SUHII-s within such 250 m buffer zone. The definitions of different urban heat island metrics are summarized in Table 1. The flowchart of this study is shown in Fig.2.

"Insert Table 1 here"

"Insert Figure 2 here"

3. Research area and Data

Urban districts of the Kowloon peninsula and Hong Kong Island across Hong Kong were selected as our study area (Fig. 3). In brief, Hong Kong is a coastal city in South China (22° 17' N, 114° 09' E), and this study area has been recognized as a compact city with high-density built-up space (Chen et al., 2012). Due to this high-rise, high-density urban environment, urban canyons have formed that influence microclimate significantly (Chen et al., 2012). In this condition, the effect of urban geometry on SUHI is complex. The observed radiometric surface temperature cannot represent the real urban surface temperature in such compact city. Thus, the SUHI based on T_c should be explored for urban climate research in Hong Kong. According to Siu and Hart (2013), the Tsak Yue Wu station (TYW) (22.40278N,114.32306E) is regarded as a representative rural station because it is surrounded by forest and far away from sea, thus was used as a reference to determine both UHI and SUHII-s. The three urban stations are at the center of the urban area and sufficiently far from the sea for the airflow to adjust to temperature in the urban area before reaching the stations, regardless of the direction. Thus, the impact of sea breeze on the UHII pattern can be neglected. The surface temperature within the 250 m buffer around the Tsak Yue Wu station was taken as the rural surface reference to calculate the SUHII.

"Insert Figure 3 here"

The radiometric temperatures retrieved from L5 / TM data in 2010 to 2011 (2010, March 26; 2010, Sep 18; 2010, December 23; 2011, June 1) and ASTER in 2013 (Mar 13, 2013, Aug 4 2013) were used in this study. Table 2 shows the observation time and dates of satellite data used in this study. Fig.4 shows the radiometric and complete surface temperature data used in this study and the retrieval method and accuracy have been described in detail by (Yang et al., 2020a). The HR thermal images of a part of the urban area of Kowloon peninsula at noon time (12:10 pm) of Oct 24 2017 (Fig.5) were collected to estimate the T_c and Tr. This area was gridded into 120 cells for further analysis. The air temperatures observed by meteorological stations in urban and rural areas at the time of the acquisition of satellite data were collected to calculate the UHII. The building data and DSM data derived by LiDAR with 1 m spatial resolution were collected to provide the building height, building height difference, building density, and sky view factor. The building height, density, building height and the sky view factor are shown in Fig. 6 and described in detail by (Yang et al., 2015).

"Insert Table 2 here"

"Insert Figure 4 here"

"Insert Figure 5 here"

"Insert Figure 6 here"

4. Results

4.1 Evaluation of different SUHIIs

4.1.1 SUHIIs from satellite data

The forest surface temperature at TYW after topographic correction was applied as a reference temperature to calculate the SUHIIs (Fig. 7). The SUHII based on radiometric surface temperature (SUHIIr) is much higher than the SUHII based on complete surface temperature (SUHIIc). The difference between SUHIIr and SUHIIc varies with building geometric conditions. In winter the difference between SUHIIr and SUHIIc in built up areas can reach 7.5 K and the mean difference was 3.7 K with standard deviation of 2.21 K when determined with the data observed by Landsat TM on Dec 23 2010. In summer this difference can reach 12 K while the mean difference was 8.0 K with standard deviation of 3.32 K when determined with the data observed by Landsat TM on Jun 1 2011. The SUHIIc can even show a cool island phenomenon, i.e. [T_c (urban) < T_c (rural)]. Generally, the latter appeared in the areas with dense buildings. The dominant factor of urban climate in daytime is solar radiation and the shadow and blockage by the buildings reduce irradiance thus reduces the surface temperature within the urban canopy. The radiometric temperature is mainly determined by the roof and street surface temperature. The high exposure of the roof surface to solar radiation helps make the roofs surface temperature much higher than wall and street. This makes the SUHIIr much higher than SUHIIc. The building shadows make the wall and street facets cooler and people may feel cooler than in rural areas without shading. This shading, combined with the thermal properties of urban materials, can result in an urban cool island. Nadir-view radiometric temperatures, with their biased view of hotter surfaces such as roofs, are less likely to capture this effect, thus the SUHII based on Tr may not detect this effect. The SUHII value is heavily affected by the selection of the rural reference, i.e. choosing some rural station with bare soil instead of vegetationas a reference, the urban cool islands may also be observed by nadir-view radiometers (Carnahan and Larson, 1990).

"Insert Figure 7 here"

The surface urban cool island conditions do not appear in night time (Fig. 8), since the longwave radiative and convective exchange within the urban space is the dominant factor. The urban surface releases energy to the atmosphere in night time by longwave emission and by convective fluxes. The atmospheric longwave radiation absorbed by the land surface during nighttime is smaller than solar irradiance during daytime, when solar irradiance is the dominant factor. The shaded facets enhance the difference between T_c and Tr during daytime. Thus, the difference between SUHIIr and SUHIIc during nighttime is much smaller than that in daytime. The maximum difference is only about 2 K and the mean difference was 0.6 K on March 13th , 2013, while the maximum difference was only about 1.5 K and the average was about 0.1 K on August, 4th 2013,. Thus, the surface urban cool island based on complete surface temperature only appears in daytime and this is similar to the UHI based on air temperature.

"Insert Figure 8 here"

4.1.2 SUHIIs from HR thermal data

The HR thermal images do not provide the surface temperature of the reference forest station. Thus we collected the land surface temperature at the location of the TYW station (LST_{TYW}) observed by Landsat / TM from 2000 to 2015 and then regressed LST_{TYW} and air temperature observed at the TYW meteorological station (Fig.9). These results show that there is very good relationship between the forest surface temperature and air temperature at TYW station, thus we used the air temperature at the same time as the HR image observation to estimate the surface temperature at the TYW station. The air temperature of TYW at 12:10 pm on Oct 24 2017 was 298.55 K and thus the forest surface temperature was 298.76 K. SUHIIr and SUHIIc were calculated using this reference temperature. Generally, SUHIIr was higher than SUHIIc. The mean SUHIIr was 10.88 K with 3.9 K standard deviation, and mean SUHIIc was 8.6 K with 4.0 K standard deviation. Since the SUHIIr is estimated using the nadir-view surface temperature, the exitance is dominated by roof and ground facets, which receive more solar irradiance at noon. Thus the SUHIIr was higher than SUHIIc. This is consistent with the results from satellite data. Since the number of SUHIIc estimates from HR is very limited, the negative value does not appear in the HR estimates of SUHII-s. The HR data (Fig.5) did show that some facets' surface temperature is lower than reference forest surface temperature. This may result in the urban cool island phenomenon.

"Insert Figure 9 here"

4.3 Impact of urban geometry on SUHIIs

We analyzed the relationship between the building density, height, SVF and building height difference and SUHIIs.

Both daytime SUHIIr and SUHIIc estimated using the Landsat TM LST retrievals are well correlated with these urban geometric parameters (Fig. 10). Results showed that the geometric parameters have different impacts on SUHIIr and SUHIIc, i.e. larger impacts on SUHIIc, while the building height and density have only slight impacts on SUHIIr. The slopes of the relationship between building height and SUHIIc are larger than that between building height and SUHIIr (Fig. 10a), thus suggesting a higher sensitivity of SUHIIc to urban geometry. The slopes of SUHIIc vs. building density are also much larger than that between SUHIIr and building density (Fig. 10b). Table 3 shows the regressions between SUHIIc, SUHIIr and geometric parameters. The SUHIIc decreases with both building height and density, because of the decrease in irradiance on wall facets and, therefore, of wall temperature, while SUHIIr has a limited sensitivity to building height and density, with building height having a larger impact on SUHIIr than building density. The latter is likely due to the increase of building height reducing the street temperature by shading, while the fractional roof cover does not change much. In this case SUHIIr decreases slightly with increasing building height, while the impact of building density on SUHIIr is barely observable. In daytime the change of SUHIIr with building density is limited, because it is the result of two contrasting effects. On the one hand, the street surface temperature decreases with increasing building density, on the other hand the fractional abundance of roof facets increases with building density, which tends to increase SUHIIr because roofs are warmer than streets. Both SUHIIc and SUHIIr increase with SVF (Figure 10c). This is because a larger SVF increases irradiance onto urban facets, thus increasing both street and wall temperature. It should be noted that SUHIIc has a higher sensitivity to SVF than SUHIIr, as shown by the slopes of the relationships in Fig. 10c. Another relevant feature is that both SUHIIc and SUHIIr decrease with building height variance (Figure 10d), i.e. with increasing shadows and aerodynamic roughness, with the latter increasing convective heat dissipation (Yang et al., 2016a). Overall, the impact of SVF and building height variance on SUHIIc is larger than the impact of building height and density on SUHIIr. A complete picture of the sensitivity of SUHIIc and SUHIIr to urban geometric parameters is provided by the slopes of the linear regressions in Table 3. Overall, the sensitivity of SUHIIc to geometric parameters is higher than SUHIIr, as shown by the larger slopes of relationships applying to SUHIIc. These results indicate that the geometry of the built – up space has a larger impact on SUHIIc than on SUHIIr, i.e. SUHIIc can represent better the difference in land surface process between urban and rural areas.

"Insert Figures 10 here"

"Insert Table 3 here"

The impact of geometric parameters on SUHII in nighttime (Fig. 11) is different than in daytime, since the dominant forcing during night time is longwave radiative and convective transfer. This mitigates the impact of urban geometry on SUHII in nighttime, although the geometry impacts on SUHIIc are still higher than that on SUHIIr. Higher building height captures more longwave radiation and reduces heat dissipation, thus increasing both SUHIIc and SUHIIr. More specifically, higher buildings lead to higher street and wall surface temperatures, which implies higher SUHIIr and SUHIIc. Like daytime, in nighttime SUHIIc is more sensitive to building height (i.e. steeper slope) than SUHIIr (Fig. 11a). In nighttime both SUHIIc and SUHIIr increase with building density (Fig. 11b), since higher building density captures better the radiative energy and reduces convective heat transfer. This increases the street and wall surface temperature, thus SUHIIc and SUHIIr. Again, SUHIIc is more sensitive to density (i.e. steeper slope) than SUHIIr (Table 3). Higher SVF increases heat dissipation by convection and longwave radiation by emission to the atmosphere, thus reducing both wall and street surface temperature, i.e. both SUHIIc and SUHIIr (Fig. 11c). The sensitivity of SUHIIs (Fig. 11c) was lower than the sensitivity of UHI_{max} to SVF (Oke et al., 2017). . This may be because roof surface temperature is insensitive to SVF and the fractional abundance of roof facets increases with decreasing SVF. The nighttime impact of building height variance on SUHIIc and SUHIIr is complex. At lower building height variance SUHIIc and SUHIIr increase slightly, then both SUHII and SUHIIr level off (Fig.11d). During nighttime the building height variance mainly affects convective heat transfer through aerodynamic roughness, which has a smoother impact than directly through irradiance in daytime. In this sense, increasing the building height difference is good for heat mitigation at daytime and nighttime when the building density cannot change.

"Insert Figures 11 here"

The dependence of is the relationships between SUHIIs on and geometric parameters has also been evaluated using the HR data (Figure 12 and Table 4). Both SUHIIr and SUHIIc increase with SVF and the slope of the relationship between SUHIIc and SVF is larger than that between SUHIIr and SVF. SUHIIr slightly increases with building density while SUHIIc decreases with building density. Both SUHIIr and SUHIIc decrease with building height and building height standard deviation or difference. The slopes of the relationship between SUHIIc and building height/building height standard deviation are larger than for SUHIIr. The results based on HR data are consistent with the ones obtained with Landsat TM data and the estimated T_c, although the number of data is limited. This means the T_c estimated by empirical relationship based on Yang et al (2020a) captures the geometric effects correctly.

"Insert Figure 12 here"

"Insert Table 4 here"

4.3 Difference between UHII and SUHIIs

To assess whether SUHIIs and UHI are related, we compared the SUHIIc and SUHIIr with UHII, which is based on air temperature (Fig. 13). Both SUHIIc and SUHIIr are positively correlated with UHI, as expected, although these correlations are relatively weak. SUHIIc values are closer to UHII's than SUHIIr's and the correlation coefficient between SUHIIc and UHII is higher than that between SUHIIr and UHII. This is because the air temperature within the urban canopy is more affected by ground and surrounding wall facets , while roof facets have very little impact on the air temperature near the ground within the urban canopy, especially for the high building (Ng et al., 2012). In this sense, T_c should be used for urban climate research, instead of Tr.

The solar zenith angle depends on Day of Year (DoY). Different solar zenith angle implies changes in irradiance and in the duration of both illumination and shadowing, leading to different values, spatial distribution and evolution of surface temperature, which are likely to result in a difference between radiometric and complete surface temperature. The solar zenith angle has been considered in the estimation of T_c from radiometric surface temperature, thus was not considered explicitly in the comparison between SUHIIs and UHII.

"Insert Figure 13 here"

5. Discussion

The difference between complete surface temperature and radiometric surface temperature has been addressed in several studies (Adderley et al., 2015; Allen et al., 2018; Jiang et al., 2018; Voogt and Oke, 1997), which documented the large difference between complete and radiometric surface temperature. This study compared the evaluation of SUHII using either nadir-viewed radiometric or complete surface temperature based on satellite thermal images and airborne high-resolution images. Results showed that SUHIIr and SUHIIc have different magnitude and spatial patterns. This is because complete and radiometric surface temperature are two different variables, although they are related (Adderley et al., 2015; Allen et al., 2018; Jiang et al., 2018; Voogt and Oke, 1997). For HR data, T_c was estimated by the facet surface temperatures from different directions and the geometric parameters were not used to estimate T_c to avoid the use of ancillary information to capture the inherent relationship between T_c and canyon geometry. For satellite data, the building geometric parameters were used since the single-view satellite data cannot provide information on different facets. Results from HR data and satellite data were consistent, however: urban geometry has different effects on SUHIIr and SUHIIc, and even some geometric parameters have contrary effects on SUHIIr and SUHIIc, because radiometric and complete surface temperature represent different facet information. This further revealed how the urban geometry determines the urban surface temperature for different components. We can say that SUHIIr and SUHIIc complement each other to understand the urban surface temperature distribution under different geometric conditions.

Considering the air temperature and surface temperature are different variables, several studies compared the UHI based on air temperature observed at meteorological stations and the radiometric surface temperature observed from satellite thermal data (Sun et al., 2015; Zhou et al., 2019), while the difference between the radiometric surface temperatures observed by nadir-viewing radiometers and complete surface temperature to estimate SUHIIs have not been evaluated. Thus, this study also compared SUHIIc and SUHIIr with UHII in Hong Kong.

The implications of our study relate to three main aspects: a) the use of observations of urban air and surface temperature in relation with the footprint of the observations; b) the interpretation of UHI, SUHIIr and SUHIIc in relation with the characteristics of the built-up space; c) expected impact of changes in urban geometry on SUHII.

For a), clearly, air and surface temperature are different geophysical variables in many ways, particularly their footprints (Oke et al., 2017). Measuring air temperature at a point captures a signal originating in the source area of the sampled air flow. The latter depends on boundary layer conditions and increases with the time of integration of the measurement. On the other hand, the footprint of a radiometric measurement of surface temperature is precisely defined by the Field of View of the instrument, and it is in general much smaller than the footprint of an air temperature measurement. This implies that the UHI and SUHI indicators convey information on the impact of the built-up space on the surface energy balance at rather different spatial scales. If information on the overall impact of the built-up environment on weather and climate is being sought, UHI meets efficiently such requirements, while a map of SUHI at high spatial resolution would require spatial averaging. Contrariwise, if a better understanding is being sought of the impact of urban geometry and materials on the thermal conditions within urban canyons at micro scale, the only viable solution is by applying SUHI detailed data.

For b), the difference between SUHIIc and SUHIIr in very dense built-up areas is larger than in flat impervious areas, because this condition makes the difference between complete and radiometric surface temperature larger than the condition of impervious flat areas. This is very obvious in Hong Kong because it is a highly compact city. Considering the buildings in Hong Kong are very high and narrow, the total wall area may even be higher than the urban horizontal surface area. Wall surface temperatures are important components of the urban climate but are under-sampled by satellite and airborne remote sensing (Hilland and Voogt, 2020). SUHIIr based on radiometric surface temperature may cause large bias in assessments of SUHI in Hong Kong.

For c), both UHI and SUHI are useful metrics to assess impacts of the design and management of urban space on urban climate and residents, including increasing the energy consumption to cool indoor spaces and heat stress on human residents in summer (Oke et al., 2017). The sensitivity of SUHIIr and SUHIIc to urban geometry, documented by our study, provides useful insights as regards: expected changes in urban climate in response to the evolution of urban space, specifically to changes in the urban geometric parameters we have considered; indications about adaptations in urban design that would contribute to mitigate the impacts of climate variability, specifically which changes in urban geometric parameters would be needed to achieve a given (target) change in SUHII-s;

Our results are preliminary and further evaluation by numerical experiments and in-situ measurements is needed but they document the sensitivity of SUHII to urban geometry.

In this context we should take into account that higher urban surface temperature may save energy for winter heating and improve the thermal comfort (Martilli et al., 2020a; Martilli et al., 2020b). Considering Hong Kong is a very densely built city with a long summer season, our results suggest that the aerodynamic roughness of the urban canopy should be increased to improve heat dissipation. The building density, height, height difference and SVF have different impacts on SUHIIr and SUHIIc. Compared with other geometric parameters, building height variance has most significant effects on SUHIIr and SUHIIc in daytime. For night time, the building height difference or variance does not lead to a significant increase in SUHIIr and SUHIIc. This means that the building height variance is an effective urban property to improve urban heat dissipation in daytime. This can be achieved by increasing the building height variance if other geometric parameters cannot be changed in Hong Kong.

The main contribution of this study is the evaluation of monitoring the SUHI using T_c instead of T_r. To this end we have used estimates of T_c with the error of estimate documented in our previous study (Yang et al., 2020a). The error of estimate may have a three-fold impact on our analyses: 1) the impact of systematic error in the estimated T_c on the assessed $SUHII_c$ and, therefore, on the comparative analysis of $SUHII_c$ and $SUHII_r$; 2) the significance of $SUHII_c$ estimates, given the random error on T_c; 3) the interpretation of the estimated RMSE, given the different nature of T_c retrievals based on Yang et al. (2020a) and the ones obtained directly from the 0.2 m x 0.2 m resolution TIR data.

As regards 1), we have used the offset (b) in the regression $T_c = aT_r + b$ (see Yang et al., 2020a for further details) as an estimate of bias on T_c, although this assumption is only applicable when a ≈1. We obtained b = 4.6 K (daytime) and b = 2.6 K (nighttime). On the other hand, the results presented in this study indicate that overall $SUHII_c < SUHII_r$, thus suggesting that the bias on T_c had a limited impact on our conclusions on $SUHII_c$ vs. $SUHII_r$. As regards 2), we have compared first the RMSE values in Yang et al. (2020a), i.e. 1.5 K(daytime) and 0.69K (nighttime) with the distributions of $SUHI_c$ either as estimated according to Yang et al. (2020a), see Fig. 14, or retrieved from the 0.2 m x 0.2 m spatial resolution data (Fig. 15). In all cases the RMSE is about 10% of the range of estimated $SUHII_c$.

Thus, the impact of such error on the estimated $SUHI_c$ is rather limited. Another aspect related to the bias on the $SUHII_c$ estimates is that a different choice of the rural reference may lead to a large bias on the values of SUHII-s (Li et al., 2020; Yao et al., 2019). This question was not investigated in this study, however.

As regards (3), it should be noted that the estimated T_c is retrieved from radiances measured with a footprint roughly 100 m in diameter, further downscaled to 30 m x 30 m in the L5/TM data products. This means that the TM instrument captures a radiance averaged over different facets within a footprint, thus filtering out inherent differences in facet surface temperature. On the contrary, the high resolution T_c is retrieved from exitance measurements of single facets, with the estimated T_c determined for each 100 m 100 m grid preserving the differences between facets and their spatial organizations within the grid. This comes close to how the model estimates (pseudo – observations) of T_c used by Yang et al. (2020a) were obtained to develop the method to estimate T_c from T_r and it implies that the RMSE given in Yang et al. (2020a) applies better to the high resolution than to the satellite retrievals of T_c. In conclusion the RMSE should be compared with the distribution of T_c and $SUHII_c$ determined with the high resolution TIR data to conclude that the impact of the error of estimate associated with the method of Yang et al. (2020a) is limited.

"Insert Figure 14 and Figure 15 here"

This study also has several limitations. For HR data, we directly used the observed facets to estimate T_c. Although we tried best to obtain all facets which were captured by the HR data of different flight-lines, there are still some facets which cannot be seen and we could not completely correct for image distortion. Both of these factors may result in a bias on estimated T_c.Though, T_c estimated from HR data can still convey more information than the nadir-view radiometric temperature. For satellite data, the main limitation is the estimation of complete surface temperature used in this study, which does not include the effects of vegetation and of variable building shape and spatial arrangement because TUF-3D only simulates the surface temperature of uniform spatial arrangements in the built-up space without vegetation. The spatial arrangement is the pattern in position, orientation and spacing of buildings. These patterns change the shadow and thermal distribution, which is likely to have an impact on the estimated difference between radiometric and complete surface temperature. In each numerical experiment with TUF – 3D the spatial arrangement of buildings must be uniform over the domain, but we performed multiple experiments by changing the arrangement of buildings.

This method estimates T_c from T_r using information on urban geometry because T_c cannot directly be observed by a nadir-looking, space-borne imaging radiometer. The estimated T_c was in a good agreement with both experimental and model reference values. In our view this shows that our T_c estimates capture the effect of urban geometry on SUHI better than T_r. The land cover and vegetation effects are not discussed in this study because the impact of these factors on SUHIIr and UHII have been studied thoroughly in previous studies.

Another limitation is the comparison of SUHIIr and SUHIIc with UHII based on station-measured air temperature. The difference between SUHI and UHI has been studied using the urban radiometric surface temperature and the air temperature observed within the urban canopy (Hu et al., 2019; Sun et al., 2015), which documented that the land cover and urban climate affect the difference between SUHIIr and UHII. Zhou et al. (2019) analyzed the rural-urban temperature variability in Israel based on different temperatures which are measured air temperature near surface, satellite-observed temperature and simulated canopy air temperature and results showed that different temperatures may lead to contrasting results, with radiometric surface temperature being dominated by the emittance of horizontal facets (Zhou et al., 2019). Although SUHIIc showed a better agreement with UHII than SUHIIr, the UHII is based on very limited measured data. We hope more air temperature measurements collected by mobile platforms can be obtained to study the geometry effects on UHII.

6. Conclusions

This study mapped the SUHII using both radiometric and complete surface temperature to document and understand the difference between SUHIIc and SUHIIr. The urban cool island effect appeared at places with denser buildings, when evaluating SUHIIc, while this effect was not captured by SUHIIr. SUHIIc is more sensitive to urban geometric parameters than SUHIIr, since geometry affects all facet temperatures, while T_r mainly captures roof and street temperature. The geometric parameters have different effects on SUHIIr and SUHIIc at daytime and nighttime and even contrary effects on SUHIIr and SUHIIc at daytime. In general, urban geometry affects more street and wall temperatures and daytime effects are larger than in nighttime. This is because the dominant factor in daytime is solar irradiance, largely controlled by building shading, while the dominant factor during nighttime is convective heat transfer. When the analysis is limited to weather conditions with calm or very light wind, the building height variance and SVF become an important determinant of SUHII. The latter is affected by geometry through aerodynamic resistance, which is a spatially smoother effect than solar irradiance. While comparing with other geometric parameters, building height variance has most significant effects on SUHIIr and SUHIIc in daytime. In night time, the building height variance does not lead to a significant increase in either SUHIIr or SUHIIc. Thus building height variance might be increased to mitigate urban heat stress if other parameters cannot be changed. Then the SUHIIc and SUHIIr were compared with UHII. Likewise SUHIIc, UHI revealed the urban cool island effect in daytime. The comparison between SUHIIs with UHII showed that the SUHIIc is much closer to UHII than SUHIIr. SUHIIc should be used for SUHI study because it captures better urban micro climate.

Acknowledgement

This work was supported by Grants by National Natural Science Foundation of China (41671430, 41901283, 41571366, 61976234, 61601522) and the Team Project of Guangdong Provincial Natural Science Foundation (2018B030312004). The authors thank the Hong Kong Planning Department, Hong Kong Lands Department, the Hong Kong Civil Engineering and Development Department, the Hong Kong Observatory and the Hong Kong Government Flying Service for the planning, building GIS, weather and climate, and airborne Lidar data, and NASA LP DAAC for the Landsat and ASTER satellite imagery. Massimo Menenti acknowledges the support of grant P10-TIC-6114 by the Junta de Andalucía and the MOST High Level Foreign Expert program (Grant nr. G20190161018) .

Conflict of Interest

The authors declare no conflict of interest.

Reference

Adderley, C., Christen, A. and Voogt, J.A., 2015. The effect of radiometer placement and view on inferred directional and hemispheric radiometric temperatures of an urban canopy. Atmos. Meas. Tech., 8(7): 2699-2714.

Allen, M., Voogt, J. and Christen, A., 2018. Time-Continuous Hemispherical Urban Surface Temperatures. Remote Sensing, 10(1): 3.

Carnahan, W.H. and Larson, R.C., 1990. An analysis of an urban heat sink. Remote Sensing of Environment, 33(1): 65-71.

Chen, L., Ng, E., An, X., Ren, C., Lee, M., Wang, U. and He, Z., 2012. Sky view factor analysis of street canyons and its implications for daytime intra-urban air temperature differentials in high-rise, high-density urban areas of Hong Kong: a GIS-based simulation approach. International Journal of Climatology, 32(1): 121-136.

Chen, X.-L., Zhao, H.-M., Li, P.-X. and Yin, Z.-Y., 2006. Remote sensing image-based analysis of the relationship between urban heat island and land use/cover changes. Remote sensing of environment, 104(2): 133-146.

Crawford, B., Krayenhoff, E.S. and Cordy, P., 2016. The urban energy balance of a lightweight low-rise neighborhood in Andacollo, Chile. Theoretical and Applied Climatology: 1-14.

Hilland, R.V.J. and Voogt, J.A., 2020. The effect of sub-facet scale surface structure on wall brightness temperatures at multiple scales. Theoretical and Applied Climatology.

Hu, L. and Brunsell, N.A., 2013. The impact of temporal aggregation of land surface temperature data for surface urban heat island (SUHI) monitoring. Remote Sensing of Environment, 134: 162-174.

Hu, Y., Hou, M., Jia, G., Zhao, C., Zhen, X. and Xu, Y., 2019. Comparison of surface and canopy urban heat islands within megacities of eastern China. ISPRS Journal of Photogrammetry and Remote Sensing, 156: 160-168.

Huang, F., Zhan, W., Voogt, J., Hu, L., Wang, Z., Quan, J., Ju, W. and Guo, Z., 2016. Temporal upscaling of surface urban heat island by incorporating an annual temperature cycle model: A tale of two cities. Remote Sensing of Environment, 186: 1-12.

Huang, X. and Wang, Y., 2019. Investigating the effects of 3D urban morphology on the surface urban heat island effect in urban functional zones by using high-resolution remote sensing data: A case study of Wuhan, Central China. ISPRS Journal of Photogrammetry and Remote Sensing, 152: 119-131.

Jiang, L., Zhan, W., Voogt, J., Zhao, L., Gao, L., Huang, F., Cai, Z. and Ju, W., 2018. Remote estimation of complete urban surface temperature using only directional radiometric temperatures. Building and Environment, 135: 224-236.

Krayenhoff, E.S. and Voogt, J., 2007. A microscale three-dimensional urban energy balance model for studying surface temperatures. Boundary-Layer Meteorology, 123(3): 433-461.

Krayenhoff, E.S. and Voogt, J.A., 2016. Daytime Thermal Anisotropy of Urban Neighbourhoods: Morphological Causation. Remote Sensing, 8(2): 108.

Kuang, W., Dou, Y., Zhang, C., Chi, W., Liu, A., Liu, Y., Zhang, R. and Liu, J., 2015. Quantifying the heat flux regulation of metropolitan land use/land cover components by coupling remote sensing modeling with in situ measurement. Journal of Geophysical Research: Atmospheres, 120(1): 113-130.

Lagouarde, J.-P., Hénon, A., Irvine, M., Voogt, J., Pigeon, G., Moreau, P., Masson, V. and Mestayer, P., 2012. Experimental characterization and modelling of the nighttime directional anisotropy of thermal infrared measurements over an urban area: Case study of Toulouse (France). Remote Sensing of Environment, 117: 19-33.

Lagouarde, J.P., Hénon, A., Kurz, B., Moreau, P., Irvine, M., Voogt, J. and Mestayer, P., 2010. Modelling daytime thermal infrared directional anisotropy over Toulouse city centre. Remote Sensing of Environment, 114(1): 87-105.

Li, J., Wang, F., Fu, Y., Guo, B., Zhao, Y. and Yu, H., 2020. A Novel SUHI Referenced Estimation Method in Multi-centers Urban Agglomeration with DMSP/OLS Nighttime Light Data. IEEE Journal of Selected Topics in Applied Earth Observations and Remote Sensing, PP: 1-1.

Li, N. and Li, X., 2020. The Impact of Building Thermal Anisotropy on Surface Urban Heat Island Intensity Estimation: An Observational Case Study in Beijing. IEEE Geoscience and Remote Sensing Letters, PP: 1-5.

Li, X., Li, W., Middel, A., Harlan, S.L., Brazel, A.J. and Turner, B.L., 2016. Remote sensing of the surface urban heat island and land architecture in Phoenix, Arizona: Combined effects of land composition and configuration and cadastral–demographic–economic factors. Remote Sensing of Environment, 174: 233-243.

Martilli, A., Krayenhoff, E.S. and Nazarian, N., 2020a. Is the Urban Heat Island intensity relevant for heat mitigation studies? Urban Climate, 31: 100541.

Martilli, A., Roth, M., Chow, W., Demuzere, M., Lipson, M., Krayenhoff, E., Sailor, D., Nazarian, N., Voogt, J., Wouters, H., Middel, A., Stewart, I., Bechtel, B., Christen, A. and Hart, M., 2020b. Summer average urban-rural surface temperature differences do not indicate the need for urban heat reduction.

Ng, E., Chen, L., Wang, Y. and Yuan, C., 2012. A study on the cooling effects of greening in a high-density city: An experience from Hong Kong. Building and Environment, 47: 256-271.

Oke, T., Cleugh, H., Grimmond, C., Schmid, H. and Roth, M., 1989. Evaluation of spatially-averaged fluxes of heat, mass and momentum in the urban boundary layer. Weather and Climate, 9: 14-21.

Oke, T.R., 1981. Canyon geometry and the nocturnal urban heat island: comparison of scale model and field observations. Journal of climatology, 1(3): 237-254.

Oke, T.R., 1982. The energetic basis of the urban heat island. Quarterly Journal of the Royal Meteorological Society, 108(455): 1-24.

Oke, T.R., Mills, G., Christen, A. and Voogt, J.A., 2017. Urban Climates.

Oke, T.R., Spronken-Smith, R.A., Jáuregui, E. and Grimmond, C.S.B., 1999. The energy balance of central Mexico City during the dry season. Atmospheric Environment, 33(24–25): 3919-3930.

Peng, S., Piao, S., Ciais, P., Friedlingstein, P., Ottle, C., Bréon, F.-M., Nan, H., Zhou, L. and Myneni, R.B., 2012. Surface Urban Heat Island Across 419 Global Big Cities. Environmental Science & Technology, 46(2): 696-703.

Roth, M., Oke, T.R. and Emery, W.J., 1989. Satellite-derived urban heat islands from three coastal cities and the utilization of such data in urban climatology. International Journal of Remote Sensing, 10(11): 1699-1720.

Shahmohamadi, P., Che-Ani, A., Ramly, A., Maulud, K. and Mohd-Nor, M., 2010. Reducing urban heat island effects: A systematic review to achieve energy consumption balance. International Journal of Physical Sciences, 5(6): 626-636.

Stewart, I.D., 2011. A systematic review and scientific critique of methodology in modern urban heat island literature. International Journal of Climatology, 31(2): 200-217.

Sun, H., Chen, Y. and Zhan, W., 2015. Comparing surface- and canopy-layer urban heat islands over Beijing using MODIS data. International Journal of Remote Sensing, 36(21): 5448-5465.

Voogt, J., 2011. Remote Sensing of Urban Surface Temperatures and the Surface Urban Heat Island.

Voogt, J.A. and Grimmond, C., 2000. Modeling surface sensible heat flux using surface radiative temperatures in a simple urban area. Journal of Applied Meteorology, 39(10): 1679-1699.

Voogt, J.A. and Oke, T., 1998. Effects of urban surface geometry on remotely-sensed surface temperature. International Journal of Remote Sensing, 19(5): 895-920.

Voogt, J.A. and Oke, T.R., 1997. Complete urban surface temperatures. Journal of Applied Meteorology, 36(9): 1117-1132.

Voogt, J.A. and Oke, T.R., 2003. Thermal remote sensing of urban climates. Remote sensing of environment, 86(3): 370-384.

Wang, D. and Chen, Y., 2019. A Geometric Model to Simulate Urban Thermal Anisotropy in Simplified Dense Neighborhoods (GUTA-Dense). IEEE Transactions on Geoscience and Remote Sensing, PP: 1-14.

Wang, D., Chen, Y., Voogt, J.A., Krayenhoff, E.S., Wang, J. and Wang, L., 2020. An advanced geometric model to simulate thermal anisotropy time-series for simplified urban neighborhoods (GUTA-T). Remote Sensing of Environment, 237: 111547.

Wang, D., Chen, Y. and Zhan, W., 2018. A geometric model to simulate thermal anisotropy over a sparse urban surface (GUTA-sparse). Remote Sensing of Environment, 209: 263-274.

Weng, Q., Lu, D. and Schubring, J., 2004. Estimation of land surface temperature–vegetation abundance relationship for urban heat island studies. Remote sensing of Environment, 89(4): 467-483.

Yang, J., Menenti, M., Krayenhoff, E.S., Wu, Z., Shi, Q. and Ouyang, X., 2019. Parameterization of Urban Sensible Heat Flux from Remotely Sensed Surface Temperature: Effects of Surface Structure. Remote Sensing, 11(11): 1347.

Yang, J., Wong, M.S., Ho, H.C., Krayenhoff, E.S., Chan, P.W., Abbas, S. and Menenti, M., 2020a. A semi-empirical method for estimating complete surface temperature from radiometric surface temperature, a study in Hong Kong city. Remote Sensing of Environment, 237: 111540.

Yang, J., Wong, M.S. and Menenti, M., 2016a. Effects of Urban Geometry on Turbulent Fluxes: A Remote Sensing Perspective. IEEE Geoscience and Remote Sensing Letters, 13(12): 1767-1771.

Yang, J., Wong, M.S., Menenti, M. and Nichol, J., 2015. Study of the geometry effect on land surface temperature retrieval in urban environment. ISPRS Journal of Photogrammetry and Remote Sensing, 109: 77-87.

Yang, J., Wong, M.S., Menenti, M., Nichol, J., Voogt, J., Krayenhoff, E.S. and Chan, P.W., 2016b. Development of an improved urban emissivity model based on sky view factor for retrieving effective emissivity and surface temperature over urban areas. ISPRS Journal of Photogrammetry and Remote Sensing, 122: 30-40.

Yang, Z., Chen, Y., Zheng, Z., Huang, Q. and Wu, Z., 2020b. Application of building geometry indexes to assess the correlation between buildings and air temperature. Building and Environment, 167: 106477.

Yao, R., Wang, L., Huang, X., Gong, W. and Xia, X., 2019. Greening in Rural Areas Increases the Surface Urban Heat Island Intensity. Geophysical Research Letters.

Yu, K., Chen, Y., Wang, D., Chen, Z., Gong, A. and Li, J., 2019. Study of the Seasonal Effect of Building Shadows on Urban Land Surface Temperatures Based on Remote Sensing Data. Remote Sensing, 11(5): 497.

Yuan, F. and Bauer, M.E., 2007. Comparison of impervious surface area and normalized difference vegetation index as indicators of surface urban heat island effects in Landsat imagery. Remote Sensing of Environment, 106(3): 375-386.

Zhan, W., Chen, Y., Voogt, J.A., Zhou, J., Wang, J., Ma, W. and Liu, W., 2012. Assessment of thermal anisotropy on remote estimation of urban thermal inertia. Remote Sensing of Environment, 123: 12-24.

Zhou, B., Kaplan, S., Peeters, A., Kloog, I. and Erell, E., 2019. “Surface,” “satellite” or “simulation”: Mapping intra-urban microclimate variability in a desert city. International Journal of Climatology, 40(6): 3099-3117.

Zhou, D., Xiao, J., Bonafoni, S., Berger, C., Deilami, K., Zhou, Y., Frolking, S., Yao, R., Qiao, Z. and Sobrino, J.A., 2018. Satellite Remote Sensing of Surface Urban Heat Islands: Progress, Challenges, and Perspectives. Remote Sensing, 11(1): 48.

Assessing the impact of urban geometry on Surface Urban Heat Island (SUHI)

Jinxin Yang[1], Massimo Menenti[3,4], Zhifeng Wu[1,2*], Man Sing Wong[5], Sawaid Abbas[5], Yong Xu[1], Qian Shi[6]

1 School of Geography and Remote Sensing, Guangzhou University, Guangzhou 510006, China；Yangjx11@gzhu.edu.cn, zfwu@gzhu.edu.cn，xu1129@gzhu.edu.cn

2 Southern Marine Science and Engineering Guangdong Laboratory (Guangzhou)，511458

3 Faculty of Civil Engineering and Earth Sciences, Delft University of Technology, P. O. Box 5048, 2600 GA Delft, Netherlands; m.menenti@tudelft.nl

4 State Key Laboratory of Remote Sensing Science, Institute of Remote Sensing and Digital Earth, Chinese Academy of Sciences, Beijing 100101, China

5 Department of Land Surveying and Geo-Informatics, The Hong Kong Polytechnic University, Kowloon, Hong Kong; email: lswong@polyu.edu.hk

6 School of Geography and Planning, Sun Yat-sen University, Guangzhou 510275, China; shixi5@mail.sysu.edu.cn

Corresponding author: Zhifeng Wu, zfwu@gzhu.edu.cn

Abbreviations

SUHIIc--The difference between the complete surface temperature of reference rural areas and the complete surface temperature of urban areas

SUHIIr--The difference between the radiometric surface temperature of reference rural areas and the radiometric surface temperature of urban areas

UHII--The difference between air temperature of reference rural station and the air temperature of urban stations

Abstract

In this study, the difference in Surface Urban Heat Island Intensity (SUHII) when using nadir-viewing radiometric and complete surface temperature (T_r and T_c) was evaluated. The urban areas of the Kowloon peninsula and Hong Kong Island across Hong Kong were selected as research area and four daytime Landsat TM data from different seasons and two nighttime ASTER data were collected to estimate the SUHII with observations of either T_r or T_c. Additionally, high spatial resolution (HR) airborne thermal images (0.2 m) observed at about 12:10 noon on Oct 24 2017 were used to retrieve T_c without additional geometric information. Results based on HR thermal data and satellite data were consistent and both retrievals of T_c indicated that the geometry of the built-up space had a larger impact on SUHII when using T_c (SUHIIc) than T_r (SUHIIr). During daytime: SUHIIc decreased with higher building density, while SUHIIr showed a very slight increase with building density. Both SUHIIc and SUHIIr decreased with higher building height but the rate of decrease of SUHIIc was higher than that of SUHIIr. Both SUHIIc and SUHIIr decreased with increasing building height difference and increased with increasing sky view factor (SVF). The rate of decrease with building height difference f SUHIIc was larger than SUHIIr. The rate of increase of SUHIIc with SVF was higher than SUHIIr. During nighttime, geometry effects on SUHIIc and SUHIIr were different from daytime. Both SUHIIc and SUHIIr increased with building density, while the rate of increase of SUHIIc with building density, as well as with building height, was much higher than that of SUHIIr. Both SUHIIc and SUHIIr decreased with SVF, but the rate of decrease of SUHIIc was higher than that of SUHIIr. Both SUHIIc and SUHIIr increased with building height difference first and then remained approximately constant. We also evaluated the UHI intensity: SUHIIc was much closer to UHII than SUHIIr. Overall, the building geometry had more significant effects on SUHIIc than on SUHIIr, i.e. SUHIIc is more representative of urban climate than SUHIIr.

Key words: urban geometry, surface urban heat island, thermal remote sensing

1. Introduction

Urbanization leads to the replacement of bare soil and vegetation by impervious surfaces, which reduces the potential for mitigation of ambient temperature through evaporation and transpiration (Kuang et al., 2015; Oke et al., 1989; Oke, 1982; Shahmohamadi et al., 2010). Instead, the radiative energy absorbed by the built-up space has to be dissipated mainly as sensible heat flux in addition to the release of anthropogenic heat, warming the surface and the atmosphere (Oke, 1981; Oke et al., 1999). This makes the urban air and surface temperature higher than the rural surface temperature because more abundant vegetation in rural areas dissipates more energy through evaporation and transpiration, thus cooling both the air and the land surface. This then has an impact on the value of both the Urban Heat Island (UHI) and Surface Urban Heat Island (SUHI) indicators of urban climate. Both UHI and SUHI have many impacts on urban climate and residents, including increasing the energy consumption for space cooling and heat stress on human residents in summer (Oke et al., 2017). The UHI metrics applies air temperature measured in the urban canopy below roof-level in the urban canyons and uses rural meteorological stations as a reference (Oke, 1981; Stewart, 2011). SUHI is defined as the difference between urban surface temperature at any urban location and the surface temperature of reference rural areas (Roth et al., 1989; Stewart, 2011). Differences between urban and rural areas in the relative magnitude of radiative and convective flux densities at the land – atmosphere interface result in different air and surface temperature in urban and rural areas, thus UHI and SUHI are indicators of the difference in surface energy balance between urban and rural areas. In other words, both UHI and SUHI are indicators of the overall effect of the built-up space on the surface energy balance.

Air and surface temperature are different geophysical variables in many ways (Oke et al., 2017) and air temperature is measured by discontinuous meteorological stations. The development of thermal infrared remote sensing made available spatially continuous observations of the land surface temperature across a range of spatial resolutions and the SUHI is based on spatially detailed observations of the radiometric surface temperature captured by space- and airborne imaging radiometers (Zhou et al., 2018). Such spatially continuous data provide detailed information towards a better understanding of urban climate and its drivers. The dependence of SUHI on urban land cover has been studied often (Chen et al., 2006; Li et al., 2016; Weng et al., 2004; Yuan and Bauer, 2007). Recently, the dependence of SUHI on the geometry of the urban built-up space has also been addressed (Yu et al., 2019). The impact of shadows determined by urban geometry has been studied by Yu et al. (2019) and results showed that in Beijing the building shadow reduced by 3.16 K the temperature of the urban impervious surface in July. More generally, the effect of urban morphology on radiometric surface temperature has been studied by Huang and Wang (2019) and the results showed that the urban geometric parameters have complex effects on the 2D and 3D pattern in urban radiometric surface temperature provided by Landsat thermal images. The urban thermal heterogeneity and 3D geometry, combined with the observation direction, lead to observe thermal anisotropy (Oke et al., 2017) and studies showed that in the Toulouse city centre the change during daytime in urban radiometric surface temperature with the view angle, i.e. the thermal anisotropy, reached 10 K on summer days in 2001 (Lagouarde et al., 2012; Lagouarde et al., 2010). This severely affects mapping of radiometric surface temperature and then the interpretation of SUHI (Hu and Brunsell, 2013; Huang et al., 2016; Li and Li, 2020; Voogt, 2011; Wang and Chen, 2019; Wang et al., 2018; Zhan et al., 2012). Current studies on SUHI are based on the radiometric surface temperature observed by thermal imaging radiometers above the urban canopy without considering the impact of anisotropy (Li et al., 2016; Peng et al., 2012; Weng et al., 2004). The radiometric surface temperature is mainly related to horizontal facets, e.g. roof and road, because most imaging radiometers are designed for nadir or near nadir looking (Roth et al., 1989; Voogt and Oke, 2003; Zhou et al. (2019)).

The impact of urban geometry on the application of thermal infrared remote sensing for urban climate research was highlighted by Roth et al (1989) and then further clarified and studied systematically by Voogt and Oke (1997, 1998, 2003) (Voogt and Oke, 1998; Voogt and Oke, 1997; Voogt and Oke, 2003). Roth et al. (1989) focused on SUHI evaluated on average for a large, mixed urbanized area using low resolution AVHRR data and discussed the limitation of the application of thermal remote sensing to study urban climate. Voogt and Oke (1997) introduced the complete surface temperature and evaluated the impact of observation geometry on measured surface temperature. Voogt and Oke (1998) documented the impact of anisotropy on the thermal infrared exitance of selected urban targets and on the surface brightness temperature retrieved from data acquired by an airborne imaging radiometer. Voogt and Oke (2003) reviewed the state of the art of thermal infrared remote sensing of urban landscapes. These studies document the notion that the complete surface temperature, which captures all the facet temperatures, is a more meaningful variable for urban climate research, since it includes information on all facets.

Different facets of the urban surface contribute to meteorological processes differently and all facets of the urban surface area are involved into the urban land surface processes and energy exchange and should be considered. The experiment conducted in Hong Kong by Ng et al. (2012) showed that a green roof is ineffective to improve thermal comfort at ground level, while trees at street level are effective in cooling pedestrian areas. This means that a roof top facet may not affect the urban canopy layer air temperature near ground, while the wall or road or other near ground facets would do so. Thus, the complete surface temperature is useful to study urban climate since it provides the information required for urban climate research, e.g. to estimate sensible heat flux (Voogt and Grimmond, 2000; Yang et al., 2019) and other heat flux densities.

SUHI is an important micro-climate indicator in urban areas. The complete surface temperature may be more useful than the radiometric surface temperature to map SUHI intensity, but it has been rarely used. The difference between complete and radiometric surface temperature can reach 10 K (Allen et al., 2018; Jiang et al., 2018; Voogt and Oke, 1997). This would lead to large differences between SUHI maps generated with either surface temperature. Thus, this study is based on the theoretical knowledge of urban geometry and it applies thermal infrared image data and complete surface temperature (Roth et al., 1989; Voogt and Oke, 1997; Voogt and Oke, 2003) to map and compare SUHIs evaluated with radiometric and (estimated) complete urban surface temperature.

In order to explore the differences in SUHIs when using different surface temperatures, this study will investigate the dependence of SUHIs on urban geometric structure when using either the complete or radiometric surface temperatures towards a better understanding of the information encapsulated in SUHI.

2. Methodology

In order to study the impact of geometry on different SUHIs, satellite data acquired by the Landsat / Thematic Map (TM) and the Advanced Spaceborne Thermal Emission and Reflection Radiometer (ASTER) and the airborne high-spatial resolution (0.2 m x 0.2 m) thermal data were collected. The satellite data of Landsat TM and ASTER were used to retrieve the radiometric surface temperature using the single channel method (Eq.1) (Yang et al., 2015) and then estimate the T_c by applying the method developed by (Yang et al., 2020a) (Eq. 2 and Eq.3):

$$E(i) = \tau_i\left[\varepsilon(\mathrm{i})B\left(T_r(i)\right) + \left(1-\varepsilon(\mathrm{i})\right)R_{at}^{\downarrow}(i)\right] + R_{at}^{\uparrow}(i) \qquad (1)$$

$E(i)$ is the radiance received by a radiometer at the top of atmosphere of pixel i. τ_i is the effective transmittance of the atmosphere, $R_{at}^{\uparrow}(i)$ is the upwelling and $R_{at}^{\downarrow}(i)$ is the downwelling atmospheric radiance. In the thermal band of L5 / TM current values of these atmospheric parameters can be obtained from the NASA Atmospheric Correction Parameter Calculator (http://atmcorr.gsfc.nasa.gov/). The radiance of ASTER AST 09T product used in this study is the ground-leaving in-band radiance including the emission of surface, the reflected radiance by the surface $\left[\varepsilon(\mathrm{i})B\left(T_r(i)\right) + \left(1-\varepsilon(\mathrm{i})\right)R_{at}^{\downarrow}(i)\right]$ and the sky thermal irradiance in band 13 of the ASTER AST 09T product can be used to calculate the downwelling radiance to retrieve the urban radiometric surface temperature (Sobrino et al, 2007). $\varepsilon(i)$is the material emissivity of pixel i, estimated as the area-weighted average of the material emissivity of component horizontal facets, e.g. roofs, roads and ground, within the footprint observed by a nadir viewing imaging radiometer (see Yang et al. (2016b) for details). $\mathrm{B}(T_r(\mathrm{i}))$ is the upwelling radiance of pixel i with radiometric temperature $T_r(i)$. $T_r(i)$ can be derived from $\mathrm{B}(T_r(\mathrm{i}))$ based on the Planck function.

The radiometric surface temperature (T_r) observed by a nadir or near-nadir viewing remote sensor over an urban canopy includes the emitted and reflected radiance from horizontal surfaces. The reflected radiance from horizontal surfaces includes a contribution from the radiance emitted by vertical surfaces that are not directly observed by nadir or near-nadir viewing remote sensors. The difference between T_r and the complete surface temperature (T_c) is caused by the urban geometry and material heterogeneity enhanced by local meteorological conditions. (Yang et al., 2020a) developed a method to estimate T_c from Tr by performing numerical experiments to generate pseudo-observations of Tr and T_c using an urban micro-climate model, i.e. the Temperatures of Urban Facets in 3-D (TUF-3D) model, This model was developed to predict urban surface temperatures under different geometric, material and meteorological conditions (Krayenhoff and Voogt, 2007). TUF-3D model has been evaluated under different neighborhood and climate conditions (Crawford et al., 2016; Krayenhoff and Voogt, 2007) and used to evaluate radiation models (Krayenhoff et al. 2014) and provide surface temperatures for remote sensing research (Krayenhoff and Voogt, 2016; Wang et al., 2020).

According to Yang et al. (2020a), the relationships between T_c and T_r can be written as:

For daytime,

$$T_c(i) = 0.913 * T_r(i) - 5.390 * \lambda_p(i) - 1.090 * \ln(F(i)) + 0.001Kn(i) - 0.013 * \theta_a(i) + 0.139 * \theta_z(i) + 20.598, \text{ with } r^2=0.97, \text{ RMSE}=1.500 \text{ K} \quad (2)$$

For nighttime,

$$T_c(i) = 0.927 * T_r(i) + 3.455 * \lambda_p(i) + 0.184 * \ln(F(i)) + 21.320, \text{ with } r^2=0.98, \text{ RMSE}=0.690 \text{ K} \quad (3)$$

$T_r(i)$ is the nadir-view radiometric surface temperature estimated according to Eq. (1), which takes also into account the geometry of the built-up space within the footprint of the radiometer, but captures the exitance of horizontal facets only, $\lambda_p(i)$ is building density, $F(i)$ is the wall area index, calculated as the ratio of wall area to horizontal area, $Kn(i)$ is the solar irradiance onto the urban canopy(Wm^{-2}), $\theta_a(i)$ is solar azimuth angle (°), $\theta_z(i)$ is solar zenith angle (°). These parameters were selected because they are the main factors that affect the difference between T_c and T_r after evaluation of the pseudo-observations mentioned above (Yang et al., 2020a).

The method developed to estimate the complete surface temperature by Yang et al. (2020a) (Eq. 2 and Eq. 3) was evaluated using a synthetic, model – based data set and results showed it can reach good accuracy (r^2=0.97, RMSE=1.50 K for daytime and r^2=0.98, RMSE=0.69 K for nighttime). The relationships developed by Yang et al. (2020a) were developed using pseudo-observations by carrying out a large number of numerical experiments with the model TUF – 3D for a wide range of key model parameters and of atmospheric forcing variables. The method of Yang et al. (2020a), therefore, is not limited to the specific conditions applying to the image data used to evaluate and demonstrate the approach.

The method to estimate the complete surface temperature developed by Yang et al. (2020a) is only applicable to urban areas with no or sparse vegetation cover, thus we only analyzed the impact of urban geometry on SUHIIs in built-up areas without vegetation. The impact of vegetation fractional cover and structure on SUHIIs will not be analyzed in this study. This study will only focus on the impacts of building geometric parameters on SUHIIs, e.g. building height, building density, Sky View Factor(SVF) and building height difference. The building density is calculated as the ratio of roof area to lot area. The SVF is calculated for all horizontal surfaces including roofs and ground. The ratio of roof to complete area and spacing of buildings may also have an impact on the relation of SUHIIr with SUHIIc. The building density, height and SVF can account for the effects of these parameters. Thus, this study chose building density, building height, SVF and building height deviation to evaluate the relation between SUHII-s and urban geometry.

The usage of T_c estimated from T_r, retrieved from TOA radiometric data acquired by space-borne imaging radiometers, is attractive because of the spatial and temporal coverage, although the spatial resolution of current observation systems is not sufficient to capture the urban landscape with sufficient detail. On the other hand, it needs to be evaluated whether the estimated T_c correctly captures the effect of urban geometry on the urban surface temperature. To this end, we have applied thermal infrared observations at 0.2 m x 0.2 m spatial resolution to determine directly T_c. These observations were acquired by a helicopter-mounted thermal camera and flight lines were in different directions to acquire multiple observations of the same target under different view angles (Figure 1). These data allowed the direct determination of T_c for a large number of urban facets.

The atmospheric and emissivity correction were conducted first by applying the thermal image process software ReseachIR provided by the Flir company (https://www.flir.cn/). The information on different facets can be obtained from different view direction (Figure 1). The HR data were gridded at 100 m x 100 m to calculate the T_c within each grid, with Tr being the temperature observed at nadir or near-nadir direction. We visually identified each facet in the grid to estimate T_c as the area-weighted mean temperature of facets observed under different directions.

"Insert Figure 1 here"

We have evaluated the two retrievals of T_c by analyzing the dependence of both retrievals on urban geometry. The relationship between SUHIIc and the urban geometry parameters was evaluated twice, i.e. using both the T_c estimated from T_r (satellite retrievals) and the T_c determined with the high resolution thermal infrared data. This objective of the evaluation was to provide insights on the impact of the two procedures to retrieve T_c on the assessment and interpretation of SUHIIc and of its dependence on urban geometry.

UHI intensity (UHII) is calculated using the air temperature observed by meteorological stations in rural and urban areas and compared with the SUHIIs based on urban radiometric and complete surface temperature. The UHII cannot be resolved with much spatial detail in this study since only a few observation stations are available, namely the three urban meteorological stations at Hong Kong Observatory (HKO), King's Park (KP) and Sham Shui Po (SSP) (Fig. 2). The mean values of SUHIIs within a 250m buffer zone around the three urban stations will be compared with UHIIs as suggested by (Yang et al., 2020b), since the highest correlation coefficient between building and air temperature was obtained when averaging the SUHII-s within such 250 m buffer zone. The definitions of different urban heat island metrics are summarized in Table 1. The flowchart of this study is shown in Fig.2.

"Insert Table 1 here"

"Insert Figure 2 here"

3. Research area and Data

Urban districts of the Kowloon peninsula and Hong Kong Island across Hong Kong were selected as our study area (Fig. 3). In brief, Hong Kong is a coastal city in South China (22° 17′ N, 114° 09′ E), and this study area has been recognized as a compact city with high-density built-up space

(Chen et al., 2012). Due to this high-rise, high-density urban environment, urban canyons have formed that influence microclimate significantly (Chen et al., 2012). In this condition, the effect of urban geometry on SUHI is complex. The observed radiometric surface temperature cannot represent the real urban surface temperature in such compact city. Thus, the SUHI based on T_c should be explored for urban climate research in Hong Kong. According to Siu and Hart (2013), the Tsak Yue Wu station (TYW) (22.40278N,114.32306E) is regarded as a representative rural station because it is surrounded by forest and far away from sea, thus was used as a reference to determine both UHI and SUHII-s. The three urban stations are at the center of the urban area and sufficiently far from the sea for the airflow to adjust to temperature in the urban area before reaching the stations, regardless of the direction. Thus, the impact of sea breeze on the UHII pattern can be neglected. The surface temperature within the 250 m buffer around the Tsak Yue Wu station was taken as the rural surface reference to calculate the SUHII.

"Insert Figure 3 here"

The radiometric temperatures retrieved from L5 / TM data in 2010 to 2011 (2010, March 26; 2010, Sep 18; 2010, December 23; 2011, June 1) and ASTER in 2013 (Mar 13, 2013, Aug 4 2013) were used in this study. Table 2 shows the observation time and dates of satellite data used in this study. Fig.4 shows the radiometric and complete surface temperature data used in this study and the retrieval method and accuracy have been described in detail by (Yang et al., 2020a). The HR thermal images of a part of the urban area of Kowloon peninsula at noon time (12:10 pm) of Oct 24 2017 (Fig.5) were collected to estimate the T_c and Tr. This area was gridded into 120 cells for further analysis. The air temperatures observed by meteorological stations in urban and rural areas at the time of the acquisition of satellite data were collected to calculate the UHII. The building data and DSM data derived by LiDAR with 1 m spatial resolution were collected to provide the building height, building height difference, building density, and sky view factor. The building height, density, building height and the sky view factor are shown in Fig. 6 and described in detail by (Yang et al., 2015).

"Insert Table 2 here"

"Insert Figure 4 here"

"Insert Figure 5 here"

"Insert Figure 6 here"

4. Results

4.1 Evaluation of different SUHIIs

4.1.1 SUHIIs from satellite data

The forest surface temperature at TYW after topographic correction was applied as a reference temperature to calculate the SUHIIs (Fig. 7). The SUHII based on radiometric surface temperature (SUHIIr) is much higher than the SUHII based on complete surface temperature (SUHIIc). The difference between SUHIIr and SUHIIc varies with building geometric conditions. In winter the difference between SUHIIr and SUHIIc in built up areas can reach 7.5 K and the mean difference was 3.7 K with standard deviation of 2.21 K when determined with the data observed by Landsat TM on Dec 23 2010. In summer this difference can reach 12 K while the mean difference was 8.0 K with standard deviation of 3.32 K when determined with the data observed by Landsat TM on Jun 1 2011. The SUHIIc can even show a cool island phenomenon, i.e. [T_c (urban) < T_c (rural)]. Generally, the latter appeared in the areas with dense buildings. The dominant factor of urban climate in daytime is solar radiation and the shadow and blockage by the buildings reduce irradiance thus reduces the surface temperature within the urban canopy. The radiometric temperature is mainly determined by the roof and street surface temperature. The high exposure of the roof surface to solar radiation helps make the roofs surface temperature much higher than wall and street. This makes the SUHIIr much higher than SUHIIc. The building shadows make the wall and street facets cooler and people may feel cooler than in rural areas without shading. This shading, combined with the thermal properties of urban materials, can result in an urban cool island. Nadir-view radiometric temperatures, with their biased view of hotter surfaces such as roofs, are less likely to capture this effect, thus the SUHII based on Tr may not detect this effect. The SUHII value is heavily affected by the selection of the rural reference, i.e. choosing some rural station with bare soil instead of vegetationas a reference, the urban cool islands may also be observed by nadir-view radiometers (Carnahan and Larson, 1990).

"Insert Figure 7 here"

The surface urban cool island conditions do not appear in night time (Fig. 8), since the longwave radiative and convective exchange within the urban space is the dominant factor. The urban surface releases energy to the atmosphere in night time by longwave emission and by convective fluxes. The atmospheric longwave radiation absorbed by the land surface during nighttime is smaller than solar irradiance during daytime, when solar irradiance is the dominant factor. The shaded facets enhance the difference between T_c and Tr during daytime. Thus, the difference between SUHIIr and SUHIIc during nighttime is much smaller than that in daytime. The maximum difference is only about 2 K and the mean difference was 0.6 K on March 13th , 2013, while the maximum difference was only about 1.5 K and the average was about 0.1 K on August, 4th 2013,. Thus, the surface urban cool island based on complete surface temperature only appears in daytime and this is similar to the UHI based on air temperature.

"Insert Figure 8 here"

4.1.2 SUHIIs from HR thermal data

The HR thermal images do not provide the surface temperature of the reference forest station. Thus we collected the land surface temperature at the location of the TYW station (LST_{TYW}) observed by Landsat / TM from 2000 to 2015 and then regressed LST_{TYW} and air temperature observed at the TYW meteorological station (Fig.9). These results show that there is very good relationship between the forest surface temperature and air temperature at TYW station, thus we used the air temperature at the same time as the HR image observation to estimate the surface temperature at the TYW station. The air temperature of TYW at 12:10 pm on Oct 24 2017 was 298.55 K and thus the forest surface temperature was 298.76 K. SUHIIr and SUHIIc were calculated using this reference temperature. Generally, SUHIIr was higher than SUHIIc. The mean SUHIIr was 10.88 K with 3.9 K standard deviation, and mean SUHIIc was 8.6 K with 4.0 K standard deviation. Since the SUHIIr is estimated using the nadir-view surface temperature, the exitance is dominated by roof and ground facets, which receive more solar irradiance at noon. Thus the SUHIIr was higher than SUHIIc. This is consistent with the results from satellite data. Since the number of SUHIIc estimates from HR is very limited, the negative value does not appear in the HR estimates of SUHII-s. The HR data (Fig.5) did show that some facets' surface temperature is lower than reference forest surface temperature. This may result in the urban cool island phenomenon.

"Insert Figure 9 here"

4.3 Impact of urban geometry on SUHIIs

We analyzed the relationship between the building density, height, SVF and building height difference and SUHIIs.

Both daytime SUHIIr and SUHIIc estimated using the Landsat TM LST retrievals are well correlated with these urban geometric parameters (Fig. 10). Results showed that the geometric parameters have different impacts on SUHIIr and SUHIIc, i.e. larger impacts on SUHIIc, while the building height and density have only slight impacts on SUHIIr. The slopes of the relationship between building height and SUHIIc are larger than that between building height and SUHIIr (Fig. 10a), thus suggesting a higher sensitivity of SUHIIc to urban geometry. The slopes of SUHIIc vs. building density are also much larger than that between SUHIIr and building density (Fig. 10b). Table 3 shows the regressions between SUHIIc, SUHIIr and geometric parameters. The SUHIIc decreases with both building height and density, because of the decrease in irradiance on wall facets and, therefore, of wall temperature, while SUHIIr has a limited sensitivity to building height and density, with building height having a larger impact on SUHIIr than building density. The latter is likely due to the increase of building height reducing the street temperature by shading, while the fractional roof cover does not change much. In this case SUHIIr decreases slightly with increasing building height, while the impact of building density on SUHIIr is barely observable. In daytime the change of SUHIIr with building density is limited, because it is the result of two contrasting effects. On the one hand, the street surface temperature decreases with increasing building density, on the other hand the fractional abundance of roof facets increases with building density, which tends to increase SUHIIr because roofs are warmer than streets. Both SUHIIc and SUHIIr increase with SVF (Figure 10c). This is because a larger SVF increases irradiance onto urban facets, thus increasing both street and wall temperature. It should be noted that SUHIIc has a higher sensitivity to SVF than SUHIIr, as shown by the slopes of the relationships in Fig. 10c. Another relevant feature is that both SUHIIc and SUHIIr decrease with building height variance (Figure 10d), i.e. with increasing shadows and aerodynamic roughness, with the latter increasing convective heat dissipation (Yang et al., 2016a). Overall, the impact of SVF and building height variance on SUHIIc is larger than the impact of building height and density on SUHIIr. A complete picture of the sensitivity of SUHIIc and SUHIIr to urban geometric parameters is provided by the slopes of the linear regressions in Table 3. Overall, the sensitivity of SUHIIc to geometric parameters is higher than SUHIIr, as shown by the larger slopes of relationships applying to SUHIIc. These results indicate that the geometry of the built – up space has a larger impact on SUHIIc than on SUHIIr, i.e. SUHIIc can represent better the difference in land surface process between urban and rural areas.

"Insert Figures 10 here"

"Insert Table 3 here"

The impact of geometric parameters on SUHII in nighttime (Fig. 11) is different than in daytime, since the dominant forcing during night time is longwave radiative and convective transfer. This mitigates the impact of urban geometry on SUHII in nighttime, although the geometry impacts on SUHIIc are still higher than that on SUHIIr. Higher building height captures more longwave radiation and reduces heat dissipation, thus increasing both SUHIIc and SUHIIr. More specifically, higher buildings lead to higher street and wall surface temperatures, which implies higher SUHIIr and SUHIIc. Like daytime, in nighttime SUHIIc is more sensitive to building height (i.e. steeper slope) than SUHIIr (Fig. 11a). In nighttime both SUHIIc and SUHIIr increase with building density (Fig. 11b), since higher building density captures better the radiative energy and reduces convective heat transfer. This increases the street and wall surface temperature, thus SUHIIc and SUHIIr. Again, SUHIIc is more sensitive to density (i.e. steeper slope) than SUHIIr (Table 3). Higher SVF increases heat dissipation by convection and longwave radiation by emission to the atmosphere, thus reducing both wall and street surface temperature, i.e. both SUHIIc and SUHIIr (Fig. 11c). The sensitivity of SUHIIs (Fig. 11c) was lower than the sensitivity of UHI_{max} to SVF (Oke et al., 2017). . This may be because roof surface temperature is insensitive to SVF and the fractional abundance of roof facets increases with decreasing SVF. The nighttime impact of building height variance on SUHIIc and SUHIIr is complex. At lower building height variance SUHIIc and SUHIIr increase slightly, then both SUHII and SUHIIr level off (Fig.11d). During nighttime the building height variance mainly affects convective heat transfer through aerodynamic roughness, which has a smoother impact than directly through irradiance in daytime. In this sense, increasing the building height difference is good for heat mitigation at daytime and nighttime when the building density cannot change.

"Insert Figures 11 here"

The dependence of is the relationships between SUHIIs on and geometric parameters has also been evaluated using the HR data (Figure 12 and Table 4). Both SUHIIr and SUHIIc increase with SVF and the slope of the relationship between SUHIIc and SVF is larger than that between SUHIIr and SVF. SUHIIr slightly increases with building density while SUHIIc decreases with building density. Both SUHIIr and SUHIIc decrease with building height and building height standard deviation or difference. The slopes of the relationship between SUHIIc and building height/building height standard deviation are larger than for SUHIIr. The results based on HR data are consistent with the ones obtained with Landsat TM data and the estimated T_c, although the number of data is limited. This means the T_c estimated by empirical relationship based on Yang et al (2020a) captures the geometric effects correctly.

"Insert Figure 12 here"

"Insert Table 4 here"

4.3 Difference between UHII and SUHIIs

To assess whether SUHIIs and UHI are related, we compared the SUHIIc and SUHIIr with UHII, which is based on air temperature (Fig. 13). Both SUHIIc and SUHIIr are positively correlated with UHI, as expected, although these correlations are relatively weak. SUHIIc values are closer to UHII's than SUHIIr's and the correlation coefficient between SUHIIc and UHII is higher than that between SUHIIr and UHII. This is because the air temperature within the urban canopy is more affected by ground and surrounding wall facets , while roof facets have very little impact on the air temperature near the ground within the urban canopy, especially for the high building (Ng et al., 2012). In this sense, T_c should be used for urban climate research, instead of Tr.

The solar zenith angle depends on Day of Year (DoY). Different solar zenith angle implies changes in irradiance and in the duration of both illumination and shadowing, leading to different values, spatial distribution and evolution of surface temperature, which are likely to result in a difference between radiometric and complete surface temperature. The solar zenith angle has been considered in the estimation of T_c from radiometric surface temperature, thus was not considered explicitly in the comparison between SUHIIs and UHII.

"Insert Figure 13 here"

5. Discussion

The difference between complete surface temperature and radiometric surface temperature has been addressed in several studies (Adderley et al., 2015; Allen et al., 2018; Jiang et al., 2018; Voogt and Oke, 1997), which documented the large difference between complete and radiometric surface temperature. This study compared the evaluation of SUHII using either nadir-viewed radiometric or complete surface temperature based on satellite thermal images and airborne high-resolution images. Results showed that SUHIIr and SUHIIc have different magnitude and spatial patterns. This is because complete and radiometric surface temperature are two different variables, although they are related (Adderley et al., 2015; Allen et al., 2018; Jiang et al., 2018; Voogt and Oke, 1997). For HR data, T_c was estimated by the facet surface temperatures from different directions and the geometric parameters were not used to estimate T_c to avoid the use of ancillary information to capture the inherent relationship between T_c and canyon geometry. For satellite data, the building geometric parameters were used since the single-view satellite data cannot provide information on different facets. Results from HR data and satellite data were consistent, however: urban geometry has different effects on SUHIIr and SUHIIc, and even some geometric parameters have contrary effects on SUHIIr and SUHIIc, because radiometric and complete surface temperature represent different facet information. This further revealed how the urban geometry determines the urban surface temperature for different components. We can say that SUHIIr and SUHIIc complement each other to understand the urban surface temperature distribution under different geometric conditions.

Considering the air temperature and surface temperature are different variables, several studies compared the UHI based on air temperature observed at meteorological stations and the radiometric surface temperature observed from satellite thermal data (Sun et al., 2015; Zhou et al., 2019), while the difference between the radiometric surface temperatures observed by nadir-viewing radiometers and complete surface temperature to estimate SUHIIs have not been evaluated. Thus, this study also compared SUHIIc and SUHIIr with UHII in Hong Kong.

The implications of our study relate to three main aspects: a) the use of observations of urban air and surface temperature in relation with the footprint of the observations; b) the interpretation of UHI, SUHIIr and SUHIIc in relation with the characteristics of the built-up space; c) expected impact of changes in urban geometry on SUHII.

For a), clearly, air and surface temperature are different geophysical variables in many ways, particularly their footprints (Oke et al., 2017). Measuring air temperature at a point captures a signal originating in the source area of the sampled air flow. The latter depends on boundary layer conditions and increases with the time of integration of the measurement. On the other hand, the footprint of a radiometric measurement of surface temperature is precisely defined by the Field of View of the instrument, and it is in general much smaller than the footprint of an air temperature measurement. This implies that the UHI and SUHI indicators convey information on the impact of the built-up space on the surface energy balance at rather different spatial scales. If information on the overall impact of the built-up environment on weather and climate is being sought, UHI meets efficiently such requirements, while a map of SUHI at high spatial resolution would require spatial averaging. Contrariwise, if a better understanding is being sought of the impact of urban geometry and materials on the thermal conditions within urban canyons at micro scale, the only viable solution is by applying SUHI detailed data.

For b), the difference between SUHIIc and SUHIIr in very dense built-up areas is larger than in flat impervious areas, because this condition makes the difference between complete and radiometric surface temperature larger than the condition of impervious flat areas. This is very obvious in Hong Kong because it is a highly compact city. Considering the buildings in Hong Kong are very high and narrow, the total wall area may even be higher than the urban horizontal surface area. Wall surface temperatures are important components of the urban climate but are under-sampled by satellite and airborne remote sensing (Hilland and Voogt, 2020). SUHIIr based on radiometric surface temperature may cause large bias in assessments of SUHI in Hong Kong.

For c), both UHI and SUHI are useful metrics to assess impacts of the design and management of urban space on urban climate and residents, including increasing the energy consumption to cool indoor spaces and heat stress on human residents in summer (Oke et al., 2017). The sensitivity of SUHIIr and SUHIIc to urban geometry, documented by our study, provides useful insights as regards: expected changes in urban climate in response to the evolution of urban space, specifically to changes in the urban geometric parameters we have considered; indications about adaptations in urban design that would contribute to mitigate the impacts of climate variability, specifically which changes in urban geometric parameters would be needed to achieve a given (target) change in SUHII-s;

Our results are preliminary and further evaluation by numerical experiments and in-situ measurements is needed but they document the sensitivity of SUHII to urban geometry.

In this context we should take into account that higher urban surface temperature may save energy for winter heating and improve the thermal comfort (Martilli et al., 2020a; Martilli et al., 2020b). Considering Hong Kong is a very densely built city with a long summer season, our results suggest that the aerodynamic roughness of the urban canopy should be increased to improve heat dissipation. The building density, height, height difference and

SVF have different impacts on SUHIIr and SUHIIc. Compared with other geometric parameters, building height variance has most significant effects on SUHIIr and SUHIIc in daytime. For night time, the building height difference or variance does not lead to a significant increase in SUHIIr and SUHIIc. This means that the building height variance is an effective urban property to improve urban heat dissipation in daytime. This can be achieved by increasing the building height variance if other geometric parameters cannot be changed in Hong Kong.

The main contribution of this study is the evaluation of monitoring the SUHI using T_c instead of T_r. To this end we have used estimates of T_c with the error of estimate documented in our previous study (Yang et al., 2020a). The error of estimate may have a three-fold impact on our analyses: 1) the impact of systematic error in the estimated T_c on the assessed $SUHII_c$ and, therefore, on the comparative analysis of $SUHII_c$ and $SUHII_r$; 2) the significance of $SUHII_c$ estimates, given the random error on T_c; 3) the interpretation of the estimated RMSE, given the different nature of T_c retrievals based on Yang et al. (2020a) and the ones obtained directly from the 0.2 m x 0.2 m resolution TIR data.

As regards 1), we have used the offset (b) in the regression $T_c = aT_r + b$ (see Yang et al., 2020a for further details) as an estimate of bias on T_c, although this assumption is only applicable when $a \approx 1$. We obtained b = 4.6 K (daytime) and b = 2.6 K (nighttime). On the other hand, the results presented in this study indicate that overall $SUHII_c < SUHII_r$, thus suggesting that the bias on T_c had a limited impact on our conclusions on $SUHII_c$ vs. $SUHII_r$. As regards 2), we have compared first the RMSE values in Yang et al. (2020a), i.e. 1.5 K(daytime) and 0.69K (nighttime) with the distributions of $SUHI_c$ either as estimated according to Yang et al. (2020a), see Fig. 14, or retrieved from the 0.2 m x 0.2 m spatial resolution data (Fig. 15). In all cases the RMSE is about 10% of the range of estimated $SUHII_c$.

Thus, the impact of such error on the estimated $SUHI_c$ is rather limited. Another aspect related to the bias on the $SUHII_c$ estimates is that a different choice of the rural reference may lead to a large bias on the values of SUHII-s (Li et al., 2020; Yao et al., 2019). This question was not investigated in this study, however.

As regards (3), it should be noted that the estimated T_c is retrieved from radiances measured with a footprint roughly 100 m in diameter, further downscaled to 30 m x 30 m in the L5/TM data products. This means that the TM instrument captures a radiance averaged over different facets within a footprint, thus filtering out inherent differences in facet surface temperature. On the contrary, the high resolution T_c is retrieved from exitance measurements of single facets, with the estimated T_c determined for each 100 m 100 m grid preserving the differences between facets and their spatial organizations within the grid. This comes close to how the model estimates (pseudo – observations) of T_c used by Yang et al. (2020a) were obtained to develop the method to estimate T_c from T_r and it implies that the RMSE given in Yang et al. (2020a) applies better to the high resolution than to the satellite retrievals of T_c. In conclusion the RMSE should be compared with the distribution of T_c and SUHII$_c$ determined with the high resolution TIR data to conclude that the impact of the error of estimate associated with the method of Yang et al. (2020a) is limited.

"Insert Figure 14 and Figure 15 here"

This study also has several limitations. For HR data, we directly used the observed facets to estimate T_c. Although we tried best to obtain all facets which were captured by the HR data of different flight-lines, there are still some facets which cannot be seen and we could not completely correct for image distortion. Both of these factors may result in a bias on estimated T_c.Though, T_c estimated from HR data can still convey more information than the nadir-view radiometric temperature. For satellite data, the main limitation is the estimation of complete surface temperature used in this study, which does not include the effects of vegetation and of variable building shape and spatial arrangement because TUF-3D only simulates the surface temperature of uniform spatial arrangements in the built-up space without vegetation. The spatial arrangement is the pattern in position, orientation and spacing of buildings. These patterns change the shadow and thermal distribution, which is likely to have an impact on the estimated difference between radiometric and complete surface temperature. In each numerical experiment with TUF – 3D the spatial arrangement of buildings must be uniform over the domain, but we performed multiple experiments by changing the arrangement of buildings.

This method estimates T_c from T_r using information on urban geometry because T_c cannot directly be observed by a nadir-looking, space-borne imaging radiometer. The estimated T_c was in a good agreement with both experimental and model reference values. In our view this shows that our T_c

estimates capture the effect of urban geometry on SUHI better than T_r. The land cover and vegetation effects are not discussed in this study because the impact of these factors on SUHIIr and UHII have been studied thoroughly in previous studies.

Another limitation is the comparison of SUHIIr and SUHIIc with UHII based on station-measured air temperature. The difference between SUHI and UHI has been studied using the urban radiometric surface temperature and the air temperature observed within the urban canopy (Hu et al., 2019; Sun et al., 2015), which documented that the land cover and urban climate affect the difference between SUHIIr and UHII. Zhou et al. (2019) analyzed the rural-urban temperature variability in Israel based on different temperatures which are measured air temperature near surface, satellite-observed temperature and simulated canopy air temperature and results showed that different temperatures may lead to contrasting results, with radiometric surface temperature being dominated by the emittance of horizontal facets (Zhou et al., 2019). Although SUHIIc showed a better agreement with UHII than SUHIIr, the UHII is based on very limited measured data. We hope more air temperature measurements collected by mobile platforms can be obtained to study the geometry effects on UHII.

6. Conclusions

This study mapped the SUHII using both radiometric and complete surface temperature to document and understand the difference between SUHIIc and SUHIIr. The urban cool island effect appeared at places with denser buildings, when evaluating SUHIIc, while this effect was not captured by SUHIIr. SUHIIc is more sensitive to urban geometric parameters than SUHIIr, since geometry affects all facet temperatures, while T_r mainly captures roof and street temperature. The geometric parameters have different effects on SUHIIr and SUHIIc at daytime and nighttime and even contrary effects on SUHIIr and SUHIIc at daytime. In general, urban geometry affects more street and wall temperatures and daytime effects are larger than in nighttime. This is because the dominant factor in daytime is solar irradiance, largely controlled by building shading, while the dominant factor during nighttime is convective heat transfer. When the analysis is limited to weather conditions with calm or very light wind, the building height variance and SVF become an important determinant of SUHII. The latter is affected by geometry through aerodynamic resistance, which is a spatially smoother effect than solar irradiance. While comparing with other geometric parameters, building height variance has most significant effects on SUHIIr and SUHIIc in daytime. In night time, the building height variance does not lead to a significant increase in either SUHIIr or SUHIIc. Thus building height variance might be increased to mitigate urban heat stress if other parameters cannot be changed. Then the SUHIIc and SUHIIr were compared with UHII. Likewise

SUHIIc, UHI revealed the urban cool island effect in daytime. The comparison between SUHIIs with UHII showed that the SUHIIc is much closer to UHII than SUHIIr. SUHIIc should be used for SUHI study because it captures better urban micro climate.

Acknowledgement

This work was supported by Grants by National Natural Science Foundation of China (41671430, 41901283, 41571366, 61976234, 61601522) and the Team Project of Guangdong Provincial Natural Science Foundation (2018B030312004). The authors thank the Hong Kong Planning Department, Hong Kong Lands Department, the Hong Kong Civil Engineering and Development Department, the Hong Kong Observatory and the Hong Kong Government Flying Service for the planning, building GIS, weather and climate, and airborne Lidar data, and NASA LP DAAC for the Landsat and ASTER satellite imagery. Massimo Menenti acknowledges the support of grant P10-TIC-6114 by the Junta de Andalucía and the MOST High Level Foreign Expert program (Grant nr. G20190161018) .

Conflict of Interest

The authors declare no conflict of interest.

Reference

Adderley, C., Christen, A. and Voogt, J.A., 2015. The effect of radiometer placement and view on inferred directional and hemispheric radiometric temperatures of an urban canopy. Atmos. Meas. Tech., 8(7): 2699-2714.

Allen, M., Voogt, J. and Christen, A., 2018. Time-Continuous Hemispherical Urban Surface Temperatures. Remote Sensing, 10(1): 3.

Carnahan, W.H. and Larson, R.C., 1990. An analysis of an urban heat sink. Remote Sensing of Environment, 33(1): 65-71.

Chen, L., Ng, E., An, X., Ren, C., Lee, M., Wang, U. and He, Z., 2012. Sky view factor analysis of street canyons and its implications for daytime intra-urban air temperature differentials in high-rise, high-density urban areas of Hong Kong: a GIS-based simulation approach. International Journal of Climatology, 32(1): 121-136.

Chen, X.-L., Zhao, H.-M., Li, P.-X. and Yin, Z.-Y., 2006. Remote sensing image-based analysis of the relationship between urban heat island and land use/cover changes. Remote sensing of environment, 104(2): 133-146.

Crawford, B., Krayenhoff, E.S. and Cordy, P., 2016. The urban energy balance of a lightweight low-rise neighborhood in Andacollo, Chile. Theoretical and Applied Climatology: 1-14.

Hilland, R.V.J. and Voogt, J.A., 2020. The effect of sub-facet scale surface structure on wall brightness temperatures at multiple scales. Theoretical and Applied Climatology.

Hu, L. and Brunsell, N.A., 2013. The impact of temporal aggregation of land surface temperature data for surface urban heat island (SUHI) monitoring. Remote Sensing of Environment, 134: 162-174.

Hu, Y., Hou, M., Jia, G., Zhao, C., Zhen, X. and Xu, Y., 2019. Comparison of surface and canopy urban heat islands within megacities of eastern China. ISPRS Journal of Photogrammetry and Remote Sensing, 156: 160-168.

Huang, F., Zhan, W., Voogt, J., Hu, L., Wang, Z., Quan, J., Ju, W. and Guo, Z., 2016. Temporal upscaling of surface urban heat island by incorporating an annual temperature cycle model: A tale of two cities. Remote Sensing of Environment, 186: 1-12.

Huang, X. and Wang, Y., 2019. Investigating the effects of 3D urban morphology on the surface urban heat island effect in urban functional zones by using high-resolution remote sensing data: A case study of Wuhan, Central China. ISPRS Journal of Photogrammetry and Remote Sensing, 152: 119-131.

Jiang, L., Zhan, W., Voogt, J., Zhao, L., Gao, L., Huang, F., Cai, Z. and Ju, W., 2018. Remote estimation of complete urban surface temperature using only directional radiometric temperatures. Building and Environment, 135: 224-236.

Krayenhoff, E.S. and Voogt, J., 2007. A microscale three-dimensional urban energy balance model for studying surface temperatures. Boundary-Layer Meteorology, 123(3): 433-461.

Krayenhoff, E.S. and Voogt, J.A., 2016. Daytime Thermal Anisotropy of Urban Neighbourhoods: Morphological Causation. Remote Sensing, 8(2): 108.

Kuang, W., Dou, Y., Zhang, C., Chi, W., Liu, A., Liu, Y., Zhang, R. and Liu, J., 2015. Quantifying the heat flux regulation of metropolitan land use/land cover components by coupling remote sensing modeling with in situ measurement. Journal of Geophysical Research: Atmospheres, 120(1): 113-130.

Lagouarde, J.-P., Hénon, A., Irvine, M., Voogt, J., Pigeon, G., Moreau, P., Masson, V. and Mestayer, P., 2012. Experimental characterization and modelling of the nighttime directional anisotropy of thermal infrared measurements over an urban area: Case study of Toulouse (France). Remote Sensing of Environment, 117: 19-33.

Lagouarde, J.P., Hénon, A., Kurz, B., Moreau, P., Irvine, M., Voogt, J. and Mestayer, P., 2010. Modelling daytime thermal infrared directional anisotropy over Toulouse city centre. Remote Sensing of Environment, 114(1): 87-105.

Li, J., Wang, F., Fu, Y., Guo, B., Zhao, Y. and Yu, H., 2020. A Novel SUHI Referenced Estimation Method in Multi-centers Urban Agglomeration with DMSP/OLS Nighttime Light Data. IEEE Journal of Selected Topics in Applied Earth Observations and Remote Sensing, PP: 1-1.

Li, N. and Li, X., 2020. The Impact of Building Thermal Anisotropy on Surface Urban Heat Island Intensity Estimation: An Observational Case Study in Beijing. IEEE Geoscience and Remote Sensing Letters, PP: 1-5.

Li, X., Li, W., Middel, A., Harlan, S.L., Brazel, A.J. and Turner, B.L., 2016. Remote sensing of the surface urban heat island and land architecture in Phoenix, Arizona: Combined effects of land composition and configuration and cadastral–demographic–economic factors. Remote Sensing of Environment, 174: 233-243.

Martilli, A., Krayenhoff, E.S. and Nazarian, N., 2020a. Is the Urban Heat Island intensity relevant for heat mitigation studies? Urban Climate, 31: 100541.

Martilli, A., Roth, M., Chow, W., Demuzere, M., Lipson, M., Krayenhoff, E., Sailor, D., Nazarian, N., Voogt, J., Wouters, H., Middel, A., Stewart, I., Bechtel, B., Christen, A. and Hart, M., 2020b. Summer average urban-rural surface temperature differences do not indicate the need for urban heat reduction.

Ng, E., Chen, L., Wang, Y. and Yuan, C., 2012. A study on the cooling effects of greening in a high-density city: An experience from Hong Kong. Building and Environment, 47: 256-271.

Oke, T., Cleugh, H., Grimmond, C., Schmid, H. and Roth, M., 1989. Evaluation of spatially-averaged fluxes of heat, mass and momentum in the urban boundary layer. Weather and Climate, 9: 14-21.

Oke, T.R., 1981. Canyon geometry and the nocturnal urban heat island: comparison of scale model and field observations. Journal of climatology, 1(3): 237-254.

Oke, T.R., 1982. The energetic basis of the urban heat island. Quarterly Journal of the Royal Meteorological Society, 108(455): 1-24.

Oke, T.R., Mills, G., Christen, A. and Voogt, J.A., 2017. Urban Climates.

Oke, T.R., Spronken-Smith, R.A., Jáuregui, E. and Grimmond, C.S.B., 1999. The energy balance of central Mexico City during the dry season. Atmospheric Environment, 33(24–25): 3919-3930.

Peng, S., Piao, S., Ciais, P., Friedlingstein, P., Ottle, C., Bréon, F.-M., Nan, H., Zhou, L. and Myneni, R.B., 2012. Surface Urban Heat Island Across 419 Global Big Cities. Environmental Science & Technology, 46(2): 696-703.

Roth, M., Oke, T.R. and Emery, W.J., 1989. Satellite-derived urban heat islands from three coastal cities and the utilization of such data in urban climatology. International Journal of Remote Sensing, 10(11): 1699-1720.

Shahmohamadi, P., Che-Ani, A., Ramly, A., Maulud, K. and Mohd-Nor, M., 2010. Reducing urban heat island effects: A systematic review to achieve energy consumption balance. International Journal of Physical Sciences, 5(6): 626-636.

Stewart, I.D., 2011. A systematic review and scientific critique of methodology in modern urban heat island literature. International Journal of Climatology, 31(2): 200-217.

Sun, H., Chen, Y. and Zhan, W., 2015. Comparing surface- and canopy-layer urban heat islands over Beijing using MODIS data. International Journal of Remote Sensing, 36(21): 5448-5465.

Voogt, J., 2011. Remote Sensing of Urban Surface Temperatures and the Surface Urban Heat Island.

Voogt, J.A. and Grimmond, C., 2000. Modeling surface sensible heat flux using surface radiative temperatures in a simple urban area. Journal of Applied Meteorology, 39(10): 1679-1699.

Voogt, J.A. and Oke, T., 1998. Effects of urban surface geometry on remotely-sensed surface temperature. International Journal of Remote Sensing, 19(5): 895-920.

Voogt, J.A. and Oke, T.R., 1997. Complete urban surface temperatures. Journal of Applied Meteorology, 36(9): 1117-1132.

Voogt, J.A. and Oke, T.R., 2003. Thermal remote sensing of urban climates. Remote sensing of environment, 86(3): 370-384.

Wang, D. and Chen, Y., 2019. A Geometric Model to Simulate Urban Thermal Anisotropy in Simplified Dense Neighborhoods (GUTA-Dense). IEEE Transactions on Geoscience and Remote Sensing, PP: 1-14.

Wang, D., Chen, Y., Voogt, J.A., Krayenhoff, E.S., Wang, J. and Wang, L., 2020. An advanced geometric model to simulate thermal anisotropy time-series for simplified urban neighborhoods (GUTA-T). Remote Sensing of Environment, 237: 111547.

Wang, D., Chen, Y. and Zhan, W., 2018. A geometric model to simulate thermal anisotropy over a sparse urban surface (GUTA-sparse). Remote Sensing of Environment, 209: 263-274.

Weng, Q., Lu, D. and Schubring, J., 2004. Estimation of land surface temperature–vegetation abundance relationship for urban heat island studies. Remote sensing of Environment, 89(4): 467-483.

Yang, J., Menenti, M., Krayenhoff, E.S., Wu, Z., Shi, Q. and Ouyang, X., 2019. Parameterization of Urban Sensible Heat Flux from Remotely Sensed Surface Temperature: Effects of Surface Structure. Remote Sensing, 11(11): 1347.

Yang, J., Wong, M.S., Ho, H.C., Krayenhoff, E.S., Chan, P.W., Abbas, S. and Menenti, M., 2020a. A semi-empirical method for estimating complete surface temperature from radiometric surface temperature, a study in Hong Kong city. Remote Sensing of Environment, 237: 111540.

Yang, J., Wong, M.S. and Menenti, M., 2016a. Effects of Urban Geometry on Turbulent Fluxes: A Remote Sensing Perspective. IEEE Geoscience and Remote Sensing Letters, 13(12): 1767-1771.

Yang, J., Wong, M.S., Menenti, M. and Nichol, J., 2015. Study of the geometry effect on land surface temperature retrieval in urban environment. ISPRS Journal of Photogrammetry and Remote Sensing, 109: 77-87.

Yang, J., Wong, M.S., Menenti, M., Nichol, J., Voogt, J., Krayenhoff, E.S. and Chan, P.W., 2016b. Development of an improved urban emissivity model based on sky view factor for retrieving effective emissivity and surface temperature over urban areas. ISPRS Journal of Photogrammetry and Remote Sensing, 122: 30-40.

Yang, Z., Chen, Y., Zheng, Z., Huang, Q. and Wu, Z., 2020b. Application of building geometry indexes to assess the correlation between buildings and air temperature. Building and Environment, 167: 106477.

Yao, R., Wang, L., Huang, X., Gong, W. and Xia, X., 2019. Greening in Rural Areas Increases the Surface Urban Heat Island Intensity. Geophysical Research Letters.

Yu, K., Chen, Y., Wang, D., Chen, Z., Gong, A. and Li, J., 2019. Study of the Seasonal Effect of Building Shadows on Urban Land Surface Temperatures Based on Remote Sensing Data. Remote Sensing, 11(5): 497.

Yuan, F. and Bauer, M.E., 2007. Comparison of impervious surface area and normalized difference vegetation index as indicators of surface urban heat island effects in Landsat imagery. Remote Sensing of Environment, 106(3): 375-386.

Zhan, W., Chen, Y., Voogt, J.A., Zhou, J., Wang, J., Ma, W. and Liu, W., 2012. Assessment of thermal anisotropy on remote estimation of urban thermal inertia. Remote Sensing of Environment, 123: 12-24.

Zhou, B., Kaplan, S., Peeters, A., Kloog, I. and Erell, E., 2019. “Surface,” “satellite” or “simulation”: Mapping intra-urban microclimate variability in a desert city. International Journal of Climatology, 40(6): 3099-3117.

Zhou, D., Xiao, J., Bonafoni, S., Berger, C., Deilami, K., Zhou, Y., Frolking, S., Yao, R., Qiao, Z. and Sobrino, J.A., 2018. Satellite Remote Sensing of Surface Urban Heat Islands: Progress, Challenges, and Perspectives. Remote Sensing, 11(1): 48.

a

b

c

d

e

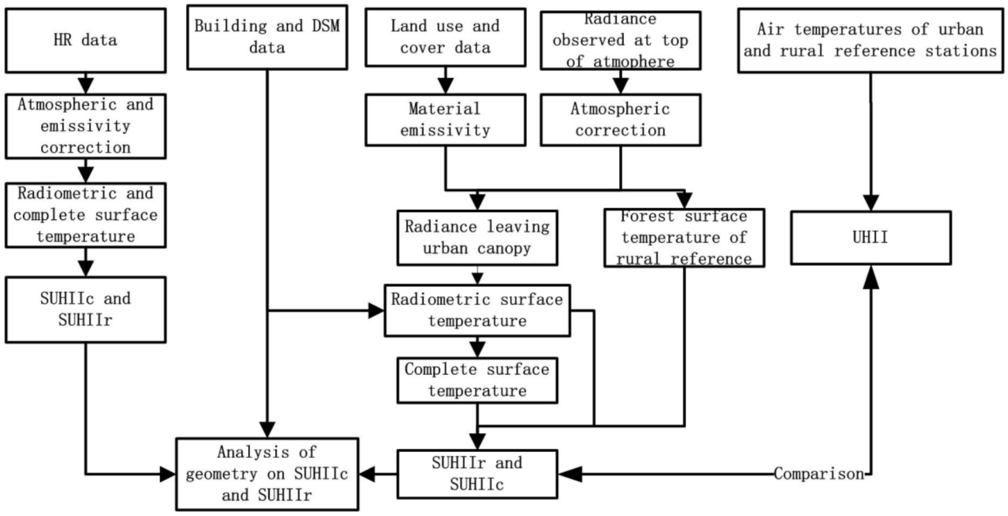

Figure 2 Flow chart of this study.

156x80mm (300 x 300 DPI)

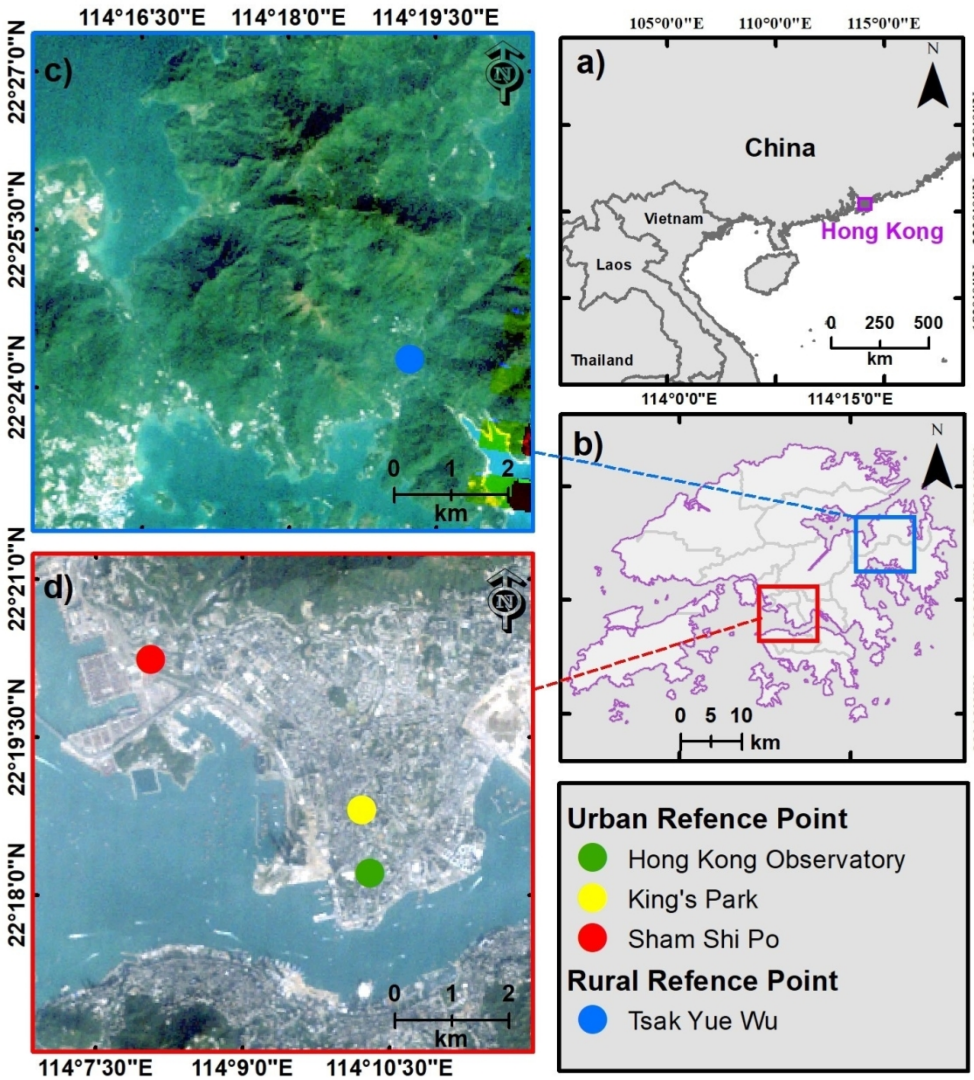

Figure 3 Study area of this study: red box in b is for c; blue box in b is for d.

385x420mm (96 x 96 DPI)

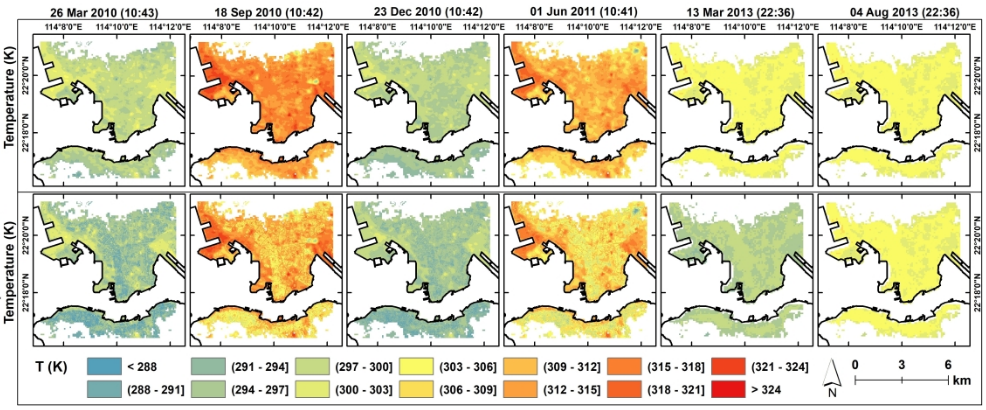

Figure 4 satellite radiometric and complete surface temperature used in this study.

1305x551mm (96 x 96 DPI)

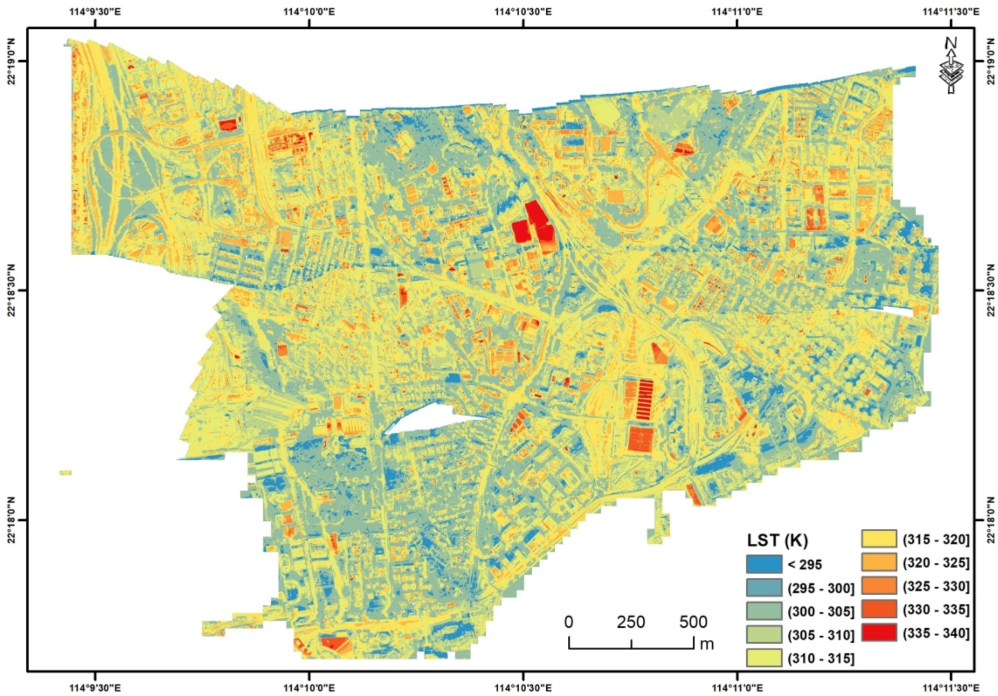

Figure 5High resolution thermal image observed at 12:10 of Oct 24 2017

636x449mm (96 x 96 DPI)

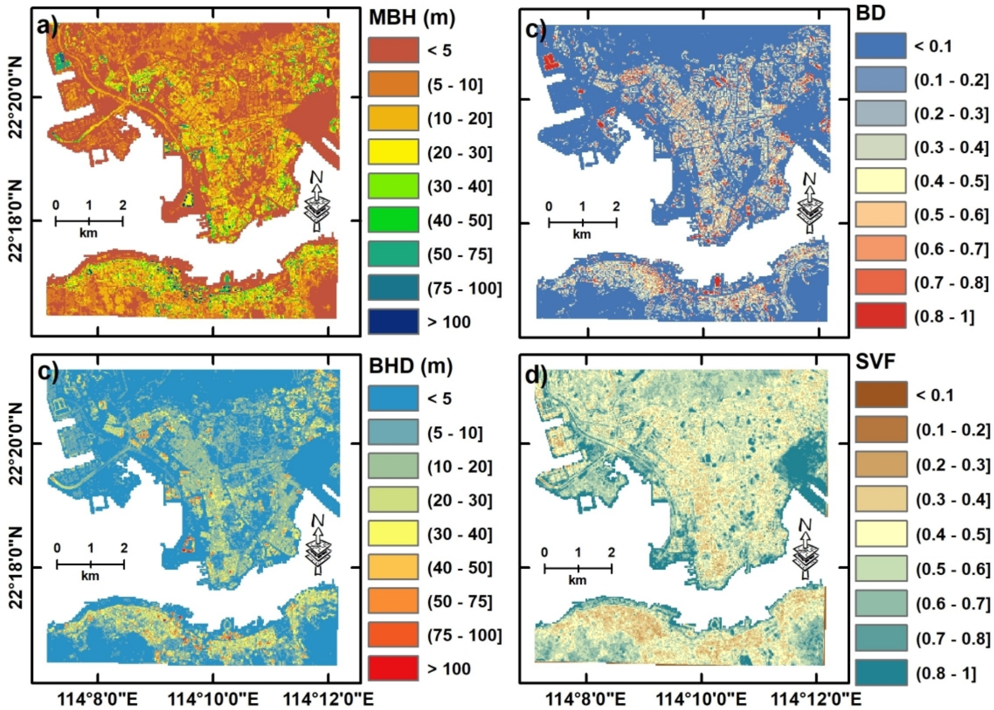

Figure 6 a, building mean height; b, building density; c, building height deviation; d, SVF.

604x432mm (96 x 96 DPI)

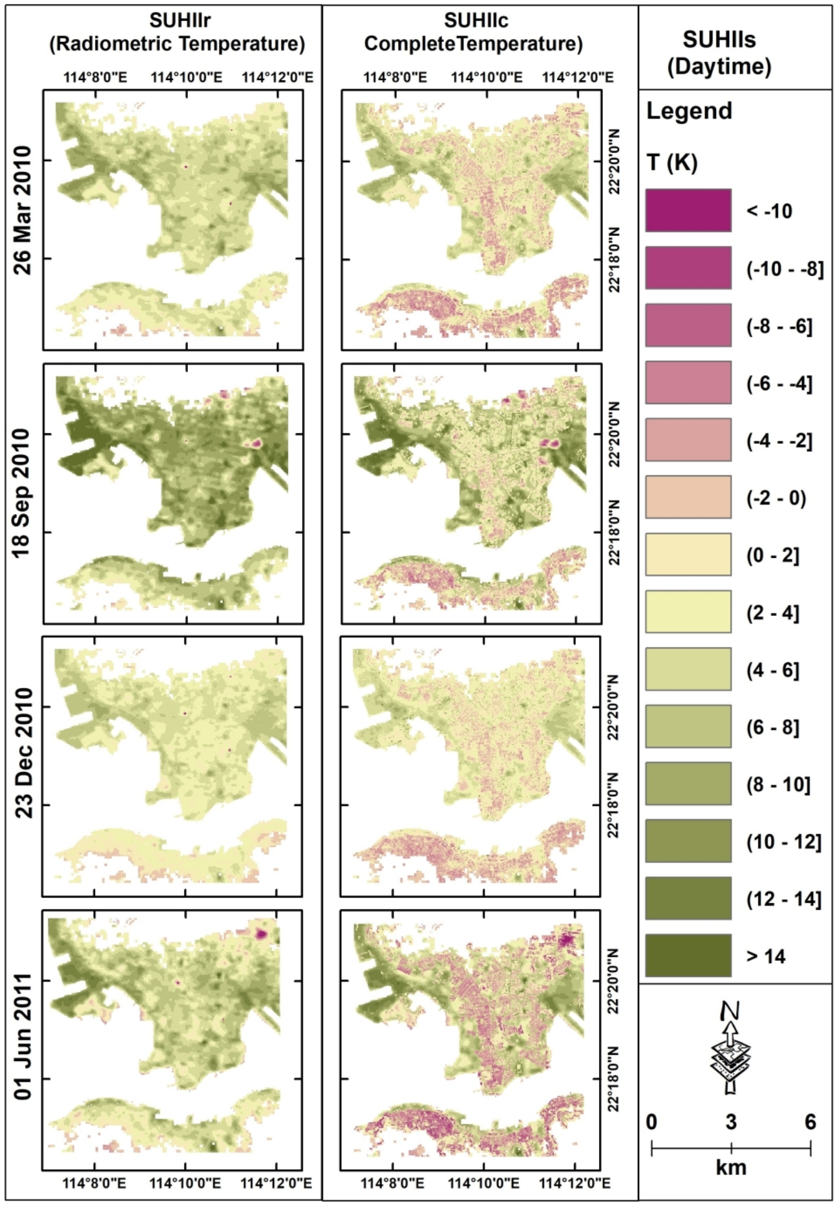

Figure 7 SUHIIs from Landsat data in the daytime

643x915mm (96 x 96 DPI)

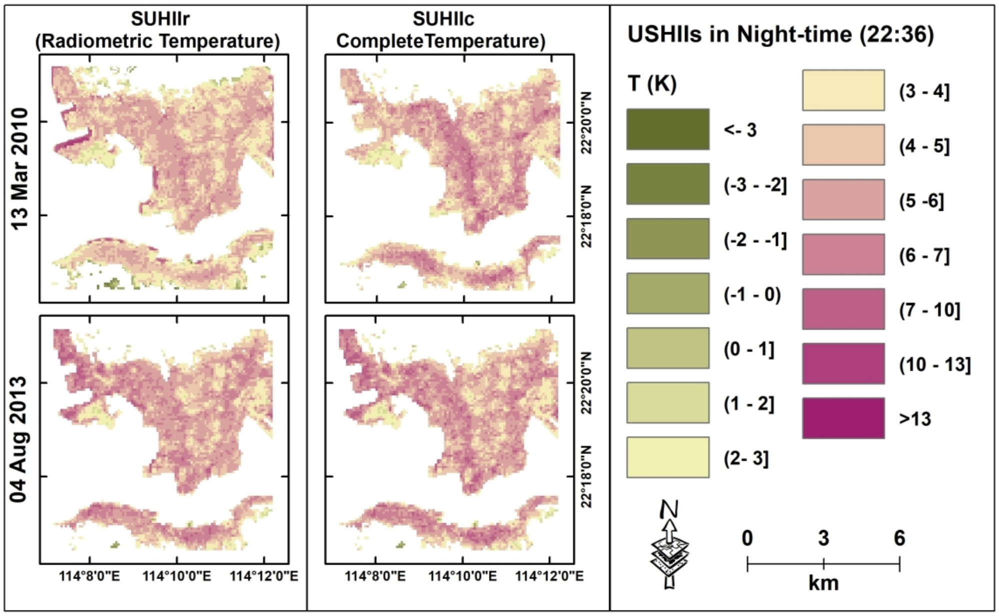

Figure 8 SUHIIs from ASTER at nighttime

797x497mm (96 x 96 DPI)

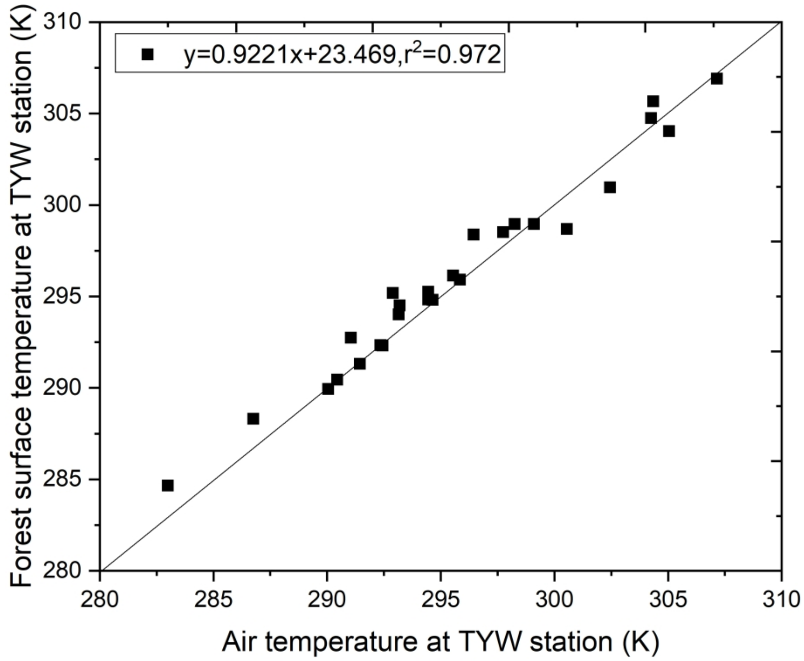

Figure 9 Relationship between air and forest surface temperature at TYW station.

272x208mm (300 x 300 DPI)

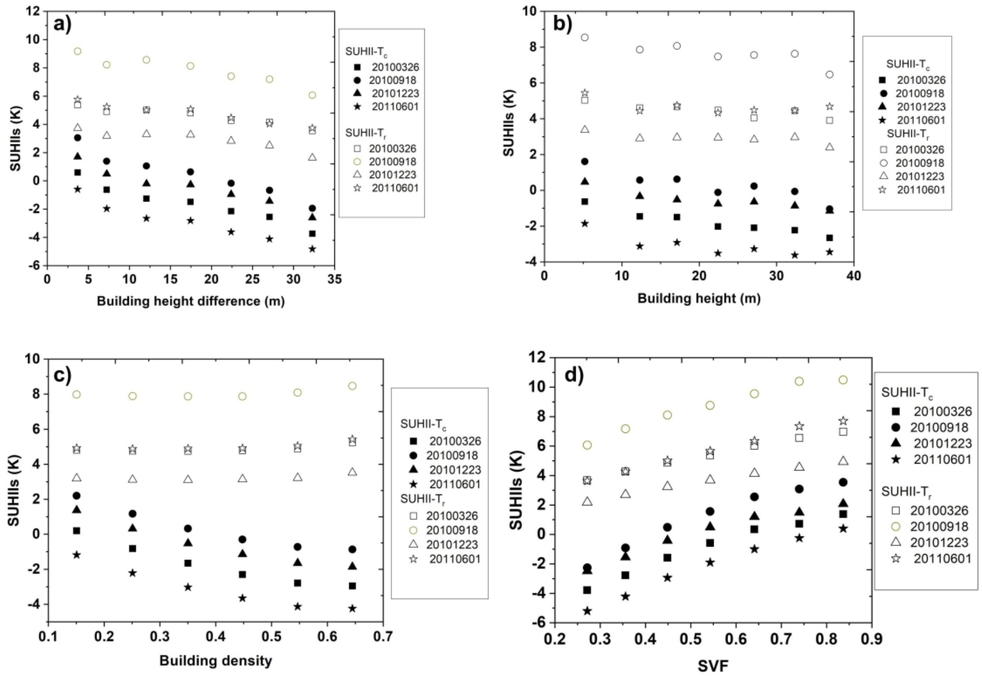

Figure 10 geometry effects on SUHIIs at daytime

835x573mm (96 x 96 DPI)

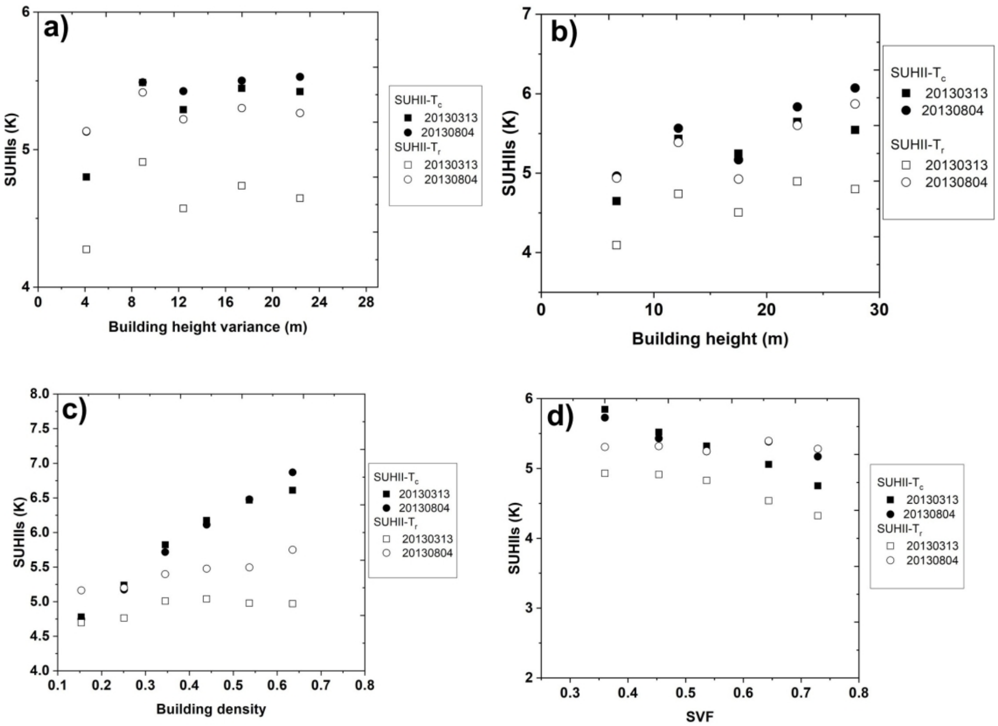

Figure 11 geometry effects on SUHIIs at nighttime.

596x438mm (96 x 96 DPI)

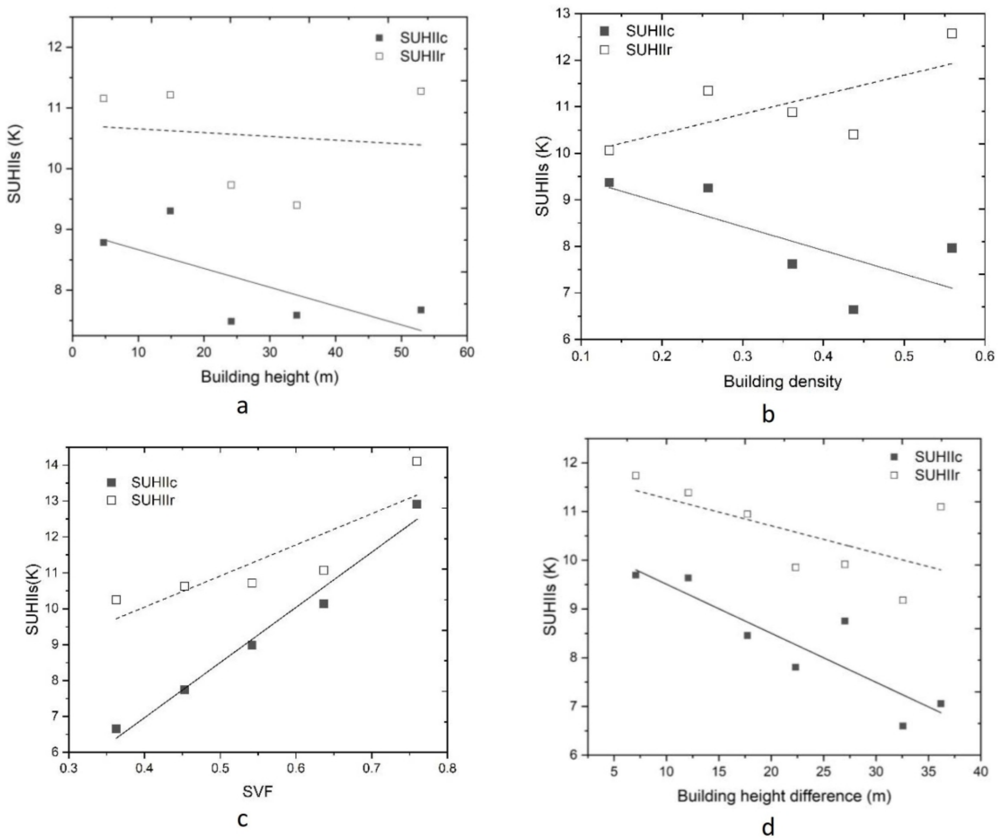

Figure 12 Relationships between SUHIIs and geometric parameters: a, SVF; b, building density; c, building height; d, building height deviation.

656x554mm (96 x 96 DPI)

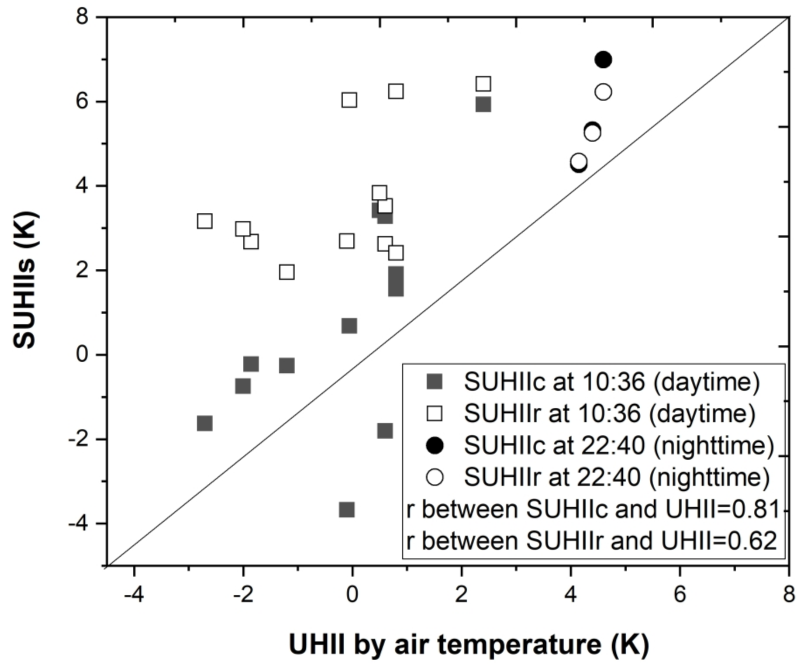

Figure 13 comparison between SUHIIs and UHI.

272x208mm (300 x 300 DPI)

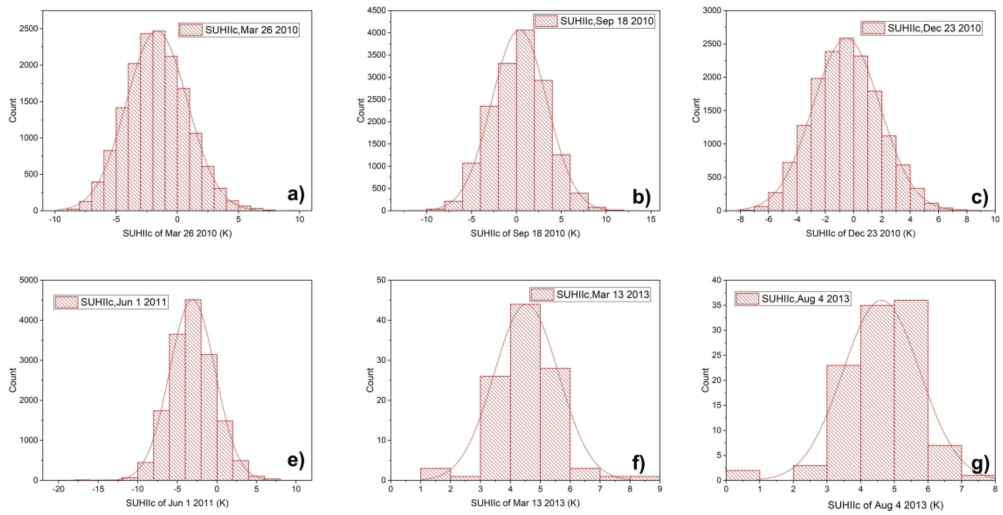

Figure 14 Frequency distribution of SUHIIc from the radiometric acquired by L8 / TIRS at 30 m x 30 m spatial resolution and ASTER at 90m x 90 m spatial resolution.

876x448mm (96 x 96 DPI)

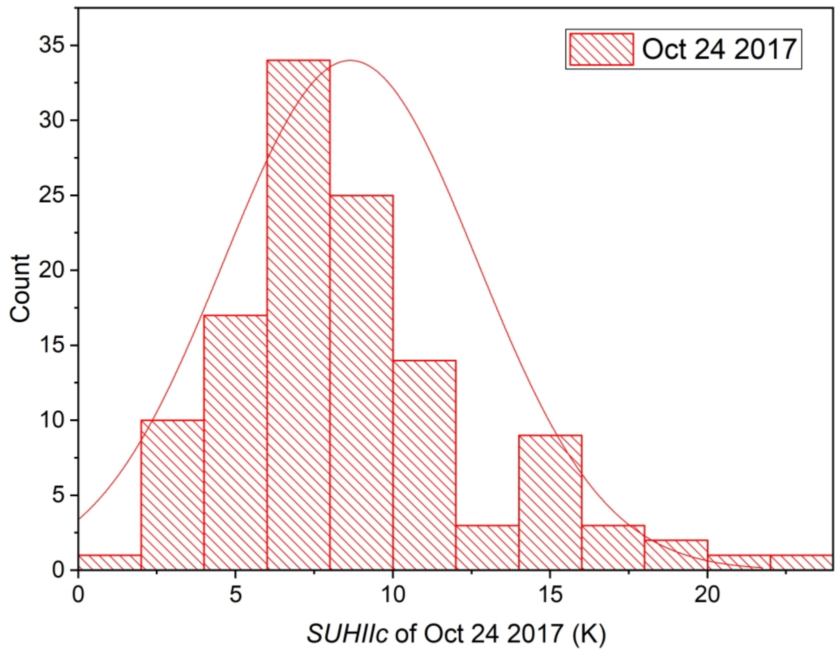

Figure 15 Frequency distribution of SUHIIc retrieved from the 0.2 m x 0.2 m spatial resolution data

271x207mm (300 x 300 DPI)

Table 1 Metrics applied in this study to evaluate the urban heat island effect.

Abbreviations	Calculation methods
SUHIIc	The difference between the surface temperature of reference rural areas and the pixel-wise complete surface temperature of urban areas
SUHIIr	The difference between surface temperature of reference rural areas and the nadir-viewed radiometric surface temperature of urban areas
UHII	The difference between air temperature of reference rural station and the air temperature of urban stations

Table 2 Satellite data used in this study.

Satellite	date	Local time
Landsat 5	2010/03/26	10:43
	2010/09/18	10:42
	2010/12/23	10:42
	2011/06/01	10:41
ASTER	2013/03/13	22:36
ASTER	2013/08/04	22:36

Table 3 Linear regression equations relating SUHIIc and SUHIIr to urban geometric parameters .

	Regression and correlation coefficients							
Date	Building density		Building height		SVF		Building height variance	
	SUHIIc	SUHIIr	SUHIIc	SUHIIr	SUHIIc	SUHIIr	SUHIIc	SUHIIr
Mar 26, 2010	y=-6.453x+0.854, r2=0.950	y=0.729x+4.583, r^2=0.531	y=-0.057x-0.543, r^2=0.941	y=-0.030x+5.120, r^2=0.77	y = 9.160x - 5.925, r^2 = 0.971	y = 5.871x + 2.171, r^2 = 0.996	y=-0.13x+0.662, r^2=0.951	y=-0.057x+5.580, r^2=0.9174
Sept 18, 2010	y=-6.278x+2.806, r^2=0.938	y=0.888x+7.677, r^2=0.497	y=-0.067x+1.729, r^2=0.846	y=-0.049x+8.750, r^2=0.76	y = 10.311x - 4.503, r^2 = 0.957	y = 7.931x + 4.3, r^2 = 0.97	y=-0.149x+3.078, r^2=0.944	y=-0.092x+9.441, r^2=0.892
Dec 23, 2010	y=-6.572x+2.040, r2=0.9534	y=0.577x+2.987, r^2=0.462	y=-0.042x+0.387, r^2=0.857	y=-0.020x+3.358, r^2=0.636	y = 8.015x - 4.2804, r^2 = 0.960	y = 4.834x + 0.978, r^2 = 0.993	y=-0.128x+1.771, r^2=0.943	y=-0.060x+3.97, r^2=0.832
Jun 1, 2011	y=-6.273x-0.575, r^2=0.9417	y=0.873x+4.673, r^2=0.596	y=-0.044x-2.140, r^2=0.671	y=-0.019x+5.080, r^2=0.3179	y = 10.016x - 7.650, r^2 = 0.9844	y = 7.410x + 1.648, r^2 = 0.995	y=-0.131x-0.654, r^2=0.947	y=-0.066x+5.916, r^2=0.945
Mar 13, 2013	y = 3.923x + 4.306 r^2 = 0.959	y = 0.607x + 4.670 r^2 = 0.581	y = 0.014x + 4.017, r^2 = 0.3406	y = 0.0055x + 3.3804 r^2 = 0.0502	y = -2.855x + 6.855 r^2 = 0.994	y = -1.7198x + 5.644 r^2 = 0.904	y = 0.027x + 4.938 r^2 = 0.459	y = 0.013x + 4.455 r^2 = 0.161
Aug 4, 2013	y = 4.438x + 4.103 r^2 = 0.995	y = 1.163x + 4.956 r^2 = 0.933	y = 0.026x + 3.848 r^2 = 0.6757	y = 0.0184x + 3.7021 r^2 = 0.407	y = -1.226x + 6.06 r^2 = 0.699	y = 0.038x + 5.290 r^2 = 0.010	y = 0.018x + 5.180 r^2 = 0.620	y = 0.0036x + 5.2207 r^2 = 0.063

Table 4 Linear regression equations relating SUHIIc and SUHIIr to urban geometric parameters of Oct 24 2017.

	Regression and correlation coefficients			
Date	Building density	Building height	SVF	Building height deviation
SUHIIr	y = 4.1839x + 9.5886 R^2 = 0.486	y = -0.0062x + 10.718 R^2 = 0.015	y = 8.6714x + 6.5776 R^2 = 0.742	y = -0.0559x + 11.827 R^2 = 0.398
SUHIIc	y = -5.0957x + 9.9511 R^2 = 0.520	y = -0.031x + 8.9774 R^2 = 0.485	y = 15.363x + 0.8214 R^2 = 0.9789	y = -0.1007x + 10.517 R^2 = 0.794